Heliyon 9 (2023) e13095

Contents lists available at ScienceDirect

Heliyon

journal homepage: www.cell.com/heliyon

Research article

Column adsorption of biological oxygen demand, chemical oxygen demand and total organic carbon from wastewater by magnetite nanoparticles-zeolite A composite

Abdulsalami Sanni Kovo [a,e], Sherifat Alaya-Ibrahim [a,e], Ambali Saka Abdulkareem [a,e], Olalekan David Adeniyi [a], Titus Chinedu Egbosiuba [b,e,*], Jimoh Oladejo Tijani [c,e], Mustapha Saheed [c,e], Blessing Onyinye Okafor [b], Yusuff Sikiru Adeyinka [d]

[a] Chemical Engineering Department, Federal University of Technology, PMB 65, Minna, Niger State, Nigeria
[b] Chemical Engineering Department, Chukwuemeka Odumegwu Ojukwu University, PMB 02, Uli Campus, Anambra State, Nigeria
[c] Chemistry Department, Federal University of Technology, Minna, PMB 65, Minna, Niger State, Nigeria
[d] Chemical and Petroleum Engineering Department, Afe Babalola University, Ado-Ekiti, Nigeria
[e] Nanotechnology Research Group, African Centre for Excellence on Mycotoxin, Federal University of Technology, PMB 65, Minna, Niger State, Nigeria

ARTICLE INFO

Keywords:
Column studies
Magnetite nanoparticles
Zeolite A
Textile wastewater
Biological oxygen demand
Chemical oxygen demand and total organic carbon

ABSTRACT

Herein, magnetite nanoparticles (NPs), zeolite A and magnetite-zeolite A (MAGZA) composite was developed by green methods. The produced nanomaterials were characterized and the effect of process parameters such as flow rate, adsorbent bed height and adsorbate inlet concentration was evaluated for the removal of biological oxygen demand (BOD), chemical oxygen demand (COD) and total organic carbon (TOC) in a column. The characterization results demonstrated the successful synthesis of magnetite NPs, zeolite A and MAGZA composite. The performance of the MAGZA composite in the fixed-bed column was superior to zeolite A and magnetite NPs. The parametric influence indicates that an increase in bed height and a decrease in the flow rate and inlet adsorbate concentration improved the performance of the adsorption column. The adsorption column demonstrated maximum performance at a flow rate (4 mL/min), bed height (5 cm) and inlet adsorbate concentration (10 mg/L). Under these conditions, the highest percent removal of BOD, COD and TOC were 99.96, 99.88 and 99.87%. Thomas and Yoon-Nelson's model suitably fitted the breakthrough curves. After five reusability cycles, the MAGZA composite demonstrated removal percent of BOD (76.5%), COD (55.5%) and TOC (64.2%). The produced MAGZA composite effectively removed BOD, COD and TOC from textile wastewater in a continuous operating mode.

* Corresponding author. Chemical Engineering Department, Chukwuemeka Odumegwu Ojukwu University, PMB 02, Uli Campus, Anambra State, Nigeria.
E-mail address: ct.egbosiuba@coou.edu.ng (T.C. Egbosiuba).

https://doi.org/10.1016/j.heliyon.2023.e13095
Received 21 July 2022; Received in revised form 11 January 2023; Accepted 16 January 2023
Available online 24 January 2023

Abbreviations

A	Area under the breakthrough curve (m^2)
APHA	American Public Health Association
BOD	Biological oxygen demand (mg/L)
COD	Chemical oxygen demand (mg/L)
TOC	Total organic carbon (mg/L)
TDS	Total dissolved solids (mg/L)
FTIR	Fourier transform infrared spectroscopy
HRTEM	High resolution scanning electron microscopy
XRD	X-ray diffractometer
BET	Brunauer- Emmett-Teller analysis
Q	Volume flow rate (mL/min)
m	Total amount of MAGZA packed inside the glass column (mg/L)
L_{MTZ}	Length of mass transfer zone (cm)
q_{eq}	Equilibrium adsorption capacity (mg/g)
q_{total}	Total amount of the adsorbed adsorbate (mg)
m_{total}	Total amount of adsorbate passed through MAGZA bed column (mg)
H	Column bed height (cm)
NPs	Nanoparticles
MAGZA	Magnetite-zeolite A composite
C_o	Adsorbate inlet concentration (mg/L)
C_t	Adsorbate outlet concentrations (mg/L)
t_b	breakthrough time (min)
t_e	breakthrough time (min)
q_o	Adsorption capacity of the column at breakthrough (mg/g)
% R	Removal percentage at breakthrough (%)
V_{eff}	The collected total volume of effluent until the point of saturation (L)
EBCT	Empty bed contact time (min)
R^2	Correlation coefficient
X^2	Chi-square
k_{Th}	Thomas kinetic model constant (mL/(min.mg))
K_{AB}	Kinetic rate constant of Adams-Bohart model (mL/min mg)
N_0	The concentration at saturation (mg/L)
u	Inlet gas linear velocity (cm/min)
k_{YN}	The kinetic constant of Yoon-Nelson model (1/min)
τ	The time required to achieve for 50% breakthrough (min)

1. Introduction

The scarcity of water in developing countries is critically challenging at the moment and on an increasing trajectory due to the increment in population, urbanization and industrialization [1,2]. Around the world, over 50% of the population does not have access to clean and safe drinking water, while about 200,000 people die annually owing to the deprivation of safe drinking water access [3]. According to the United Nations (UN) water report, over 2.3 billion people are living in water-stressed countries, out of which 733 million are living in higher and more perilous water-stressed countries [4]. To achieve overall access to clean, affordable and sustainable water resources for all by 3020, the UN inaugurated a clean water and sanitation initiative under the sustainable development goals (SDGs). However, the recorded progress had been slow and more than 80% of the generated wastewater from human activities in industries is currently discharged into the environment, rivers and seas without undergoing treatment techniques [4]. Among the industries, the textile industry has been reported as one of the industries consuming a large amount of water, dyes, additives, organic and inorganic chemicals during the manufacturing process [5,6]. Therefore, textile wastewater generally contains organic compounds and pollutants that enhance toxicity, biological oxygen demand (BOD), chemical oxygen demand (COD) and total organic carbon (TOC) [7–9]. Due to the serious environmental pollution, water resource contamination and the associated health problems caused by these pollutants, their removal from wastewater remains a popular topic.

Owing to the increasing demand for environmental protection, several conventional treatment methods have been reported by researchers to effectively remove pollutants from wastewater. For instance, ion exchange [10], reverse osmosis [11], nanofiltration [12], biological technique [13], coagulation/flocculation [14], reverse osmosis [15], chemical precipitation [16], photocatalysis [17, 18], membrane processes [19], advanced oxidation processes [8] and adsorption process [20]. However, some of the highlighted methods have their limitations that are either require frequent maintenance, high cost of operation, longer degradation time,

generation of sludge in large amounts and the use of expensive chemicals [21,22]. In recent times, adsorption had gained popularity in the removal of organic pollutants and heavy metals in wastewater which was ascribed to its low cost, high removal effectiveness, operation ease and readily available numerous adsorbent materials [23,24]. Notably, the cost of the adsorption technique and its efficiency is highly dependent on the material.

Before now, classical adsorbents namely: zeolites [25], synthetic resins [26], biowastes [27], biochar [28] and poly (methyl methacrylate) [29] have been randomly used to decontaminate wastewater. Generally, zeolites are aluminosilicate minerals that are hydrated to be in a microporous structure and used extensively as adsorbent material to remove hazardous contaminants from wastewater [30,31]. However, zeolites and the other identified adsorbents are limited by the difficulty in their separation process. As such, nanoparticles and nanomaterials had been attracting special attention due to their biocompatibility, chemical stability, efficacy in the separation process, higher adsorption efficiency and strength in the suspension medium [32]. Some nanoparticles and their composites such as iron nanoparticles (NPs) [33], nickel NPs [34], cobalt NPs [35], Fe_3O_4 graphene biochar composite [36], graphite nickel NPs composite [37], nickel NPs multiwalled carbon nanotubes [32], treated and functionalized carbon nanotubes [38], cobalt NPs activated carbon composite [39], iron NPs graphene oxide chitosan composite [40], silver nanoparticles-carbon nanotubes composites [41] and zero-valent iron/zeolite composite [42] have been prepared for the removal of both organic and inorganic pollutants from industrial wastewater.

Among them, magnetite-zeolite composite has been prepared previously to treat wastewater, for instance, Du et al. [36] reported the removal of cadmium ions in a batch adsorption system using modified zeolite-supported nanoscale zero-valent iron composites. In another study, iron-oxide nanoparticles decorated zeolite nanocomposite were covered with ionic liquid for the catalytic reduction and degradation of 2-nitroaniline, 3-nitroaniline, 4-nitroaniline, Nitrophenyl diamine and dyes (Methylene blue and Allura red) [43]. Also, NaA zeolite-coated nanoparticles (NZCMNs) were prepared and investigated for the removal of Pb (II) and Cu (II) ions from aqueous solutions [44]. In 2020, Xu et al. [45] investigated the adsorption capacity of ammonia and phosphate using green synthesized iron oxide nanoparticles dispersed onto zeolite. In addition, iron-based NPs-zeolite composites were also examined for the adsorption of caesium from aqueous solutions in a batch mode [46]. Remarkably, the application of NPs embedded nanocomposites in adsorption studies is becoming attractive due to the enhanced chemical, catalytic, mechanical and optical [1]. To the best of our knowledge, no study has been found to examine the fixed-bed adsorption of BOD, COD and TOC from textile wastewater using a composite of magnetite NPs (prepared using *Mangifera indica* leaves) and zeolite A.

Overall, much attention has been given to the biosynthesis of NPs using an extract from plant and agricultural waste due to their cost-effectiveness, simplicity, availability and eco-friendly method [47]. This study focused on the green synthesis-assisted fabrication of magnetite NPs (Fe_3O_4) using *Mangifera indica* leaves extract which contains a high quantity of polyphenolic compounds that functions as a reducing and capping agent. In this study, zeolite A was prepared from Ahoko clay and the composite of magnetite NPs and zeolite A fabricated. Typically, the prepared magnetite NPs, zeolite A and magnetite NPs-zeolite A composite were characterized using Fourier transform infrared (FTIR) spectroscopy, X-ray diffraction (XRD), high-resolution transmission electron microscopy (HRTEM) and Braunauer Emmett Teller (BET), The fixed-bed adsorption capacities of magnetite NPs, zeolite A and magnetite NPs-zeolite A composite towards BOD, COD and TOC were compared, while further application of the magnetite NPs-zeolite A composite was explored in detail targeting organic pollutants at different conditions of flow rate, adsorbent bed height and initial adsorbate concentration. Thereafter, the breakthrough analysis was conducted using Thomas, Adams-Bohart and Yoon-Nelson models. The reusability study of the magnetite NPs-zeolite A composite and the comparative investigation of the adsorbent material with the literature were also examined.

2. Materials and methods

2.1. Materials

The analytical grade chemicals used in this study such as iron (III) chloride hexahydrate ($FeCl_3.6H_20$), iron (II) chloride tetrahydrate ($FeCl_2.4H_20$), potassium chloride (KCl), sulfuric acid (H_2SO_4), hydrochloric acid (HCl) and sodium hydroxide (NaOH) powder were in the purity range 96–99.8% and purchased from Sigma Aldrich, Lagos. The chemicals were not purified before use. Deionized water was provided by the Milli-Q system and applied for the aqueous solutions preparations. The kaolin clay used was obtained from Ahoko, Kogi state, Nigeria. Also, mango leaves used in this study were collected from the premises of the Federal University of Technology, Minna. The textile wastewater effluent was collected from Unique Tie and Dye textile Industry in Ilorin, Kwara State, Nigeria and was analyzed at the Regional Water Quality Laboratory, Federal Ministry of Water Resources, Minna, Niger State, Nigeria.

2.2. Preparation of magnetite nanoparticles

Herein, the biosynthesis of magnetite nanoparticles was achieved using *Mangifera indica* (mango) leaf extract. Initially, the *Mangifera indica* leaves were meticulously washed to remove dirt using distilled water and dried at room temperature for 14 days in the absence of direct sunlight. Thereafter, the dried *Mangifera indica* leaves were reduced in size using a porcelain mortar and pestle. Then, 20 g of the powdered *Mangifera indica* leaves were added to a 500 mL conical flask containing 200 mL of deionized water and boiled for 15 min on a magnetic stirrer (300 rpm). In the end, the mixture was allowed to cool to ambient temperature, followed by centrifugation at 6600 rpm for 30 min, decantation and filtration using Whatman No. 1 filter paper. The filtrate (*Mangifera indica* leaf extract) was labelled MIL extract and stored in an airtight bottle at 4 °C until further use.

For the synthesis of magnetite using the prepared ML extract, 0.324 g and 0.199 g of $FeCl_3.6H_2O$ and $FeCl_2.4H_20$ of 0.01 M were

weighed and dissolved in 100 mL of deionized water contained in an Erlenmeyer flask of 250 mL and placed on a magnetic stirrer at 50 °C. Afterwards, 10 mL of MIL extract was added to the iron chloride solution under sustained stirring (300 rpm) for 30 min. A colour change from brown to dark red was observed which indicated the formation of magnetite nanoparticles (NPs). In addition to the observed colour change, UV–visible spectroscopy was used to confirm the formation of the magnetite NPs. Subsequently, the sample was oven-dried at 105 °C for 12 h before calcination at 400 °C for 6 h. The obtained magnetite NPs was stored in an airtight container until further application.

2.3. Preparation of zeolite A

In this study, the beneficiation, metakaolinization and preparation of zeolite A were carried out by modifying the method reported elsewhere [48]. Briefly, the Ahoko clay was ground to powder using an electric blender, soaked in distilled water and allowed to settle in an aspirator bottle before decantation, oven drying and calcination at 600 °C for 1 h to obtain metakaolin. A typical synthesis of zeolite A was achieved by adding 6 g of metakaolin into a solution of NaOH (4 g) powder and distilled water (30 mL) in a beaker (250 mL). Thereafter, a magnetic stirrer was used to age the resulting gel at room temperature for 6 h, before crystallization in a stainless autoclave at 100 °C for 90 min. Subsequent cooling to room temperature was allowed, followed by washing with distilled water until a pH close to 7 was obtained. In the end, the obtained zeolite A was dried in an oven at 105 °C for 10 h and safely stored in an airtight bottle until future application.

2.4. Preparation of magnetite NPs incorporated zeolite A

For the preparation of magnetite NPs incorporated zeolite A, 10 g of magnetite NPs was added to a conical flask of 250 mL containing 50 mL of deionized water. Thereafter, 5 g zeolite A of was added to the slurry and placed in the ultrasonic bath (SB25-12DT, Ultrasonic Scientz) at 50 °C for 6 h to ensure molecular incorporation homogeneity and bond cleavages by sound waves. Above all, the composite was dried in an oven for 2 h and the obtained magnetite NPs incorporated zeolite A was labelled MAGZA composite and stored in an airtight bottle until further characterization and application for the removal of BOD, COD and TOC from textile wastewater.

2.5. Analytical methods

The microstructure of the prepared magnetite NPs, zeolite A and MAGZA composite was analyzed using high-resolution transmission electron microscopy (HRTEM, Zeiss Auriga, UK). To evaluate the porous characteristics of the materials, Braunauer Emmett Teller (BET, NOVA 4200, UK) was used. For the determination of the functional groups present on the magnetite NPs, zeolite A and MAGZA composite, Fourier transform infrared (FTIR, PerkinElmer, UK) spectroscopy was used at the spectrum range of 500–4000 cm^{-1}. The crystalline nature of the materials was examined using X-ray diffraction (XRD, 6000, Shimadzu Scientific) analysis.

Further analytical techniques were conducted to determine the water quality parameters such as biological oxygen demand (BOD) and chemical oxygen demand (COD) using standard methods [49]. Briefly, the BOD analysis before and after treatment was conducted using a 5-day BOD test (5210 B) by closed reflux technique in BOD bottles of 300 mL containing the textile wastewater and covered with an airtight seal [49]. Several dilutions and seeding were performed and samples were poured into two BOD bottles. The initial dissolved oxygen (DO) of one of the bottles was analyzed, while the second bottle was incubated for 5 days at 20 °C. At the end of the 5 days, the measurement of the final DO was taken [8,49–51]. The percentage adsorption of BOD was evaluated using Eq. S1 (Supplementary material).

The analysis for the COD before and after treatment by closed reflux technique. In brief, a diluted sample of 3 mL was mixed with potassium dichromate ($K_2Cr_2O_7$) of 2 mL and digestion acid (sulfuric acid) of 4 mL. Thereafter, the mixture was digested in a Hach COD digester for 2 h at 150 °C [49,51–53]. The COD was measured using HACH DR 2800 spectrophotometer, while the percentage adsorption of COD was calculated using Eq. S2 (Supplementary Material).

The TOC was also evaluated using a TOC analyzer (Shimadzu, Japan) by the 5220 B-open reflux method [8,49,50]. The removal percentage of TOC was evaluated using Eq. S3 (Supplementary material). The analysis of other water quality parameters like total organic carbon (TOC), total dissolved solids (TDS), conductivity, turbidity, total alkalinity, nitrate, ammonia, chloride, phosphate, fluoride and sulphate were conducted before and after treatment to reduce the pollutants below the permissible concentrations recommended by World Health Organization [54] and US Environmental Protection Agency [55] using APHA standards [49,51]. Also, the heavy metal ions (iron, chromium, nickel, zinc, lead, cadmium, copper and manganese) concentrations before and after treatment were determined using Atomic Absorption Spectrophotometer (AAS) (PG 990, UK).

2.6. Selectivity of adsorbents

In the first place, the selective adsorption of BOD, COD and TOC on the magnetite NPs, zeolite A and MAGZA composite was investigated at the flow rate of 4 mL/min, adsorbent bed height of 4 cm and adsorbate inlet concentration of 20 mg/L, respectively. Herein, a constant pH of 7 was maintained using 1 M of H_2SO_4/NaOH at an ambient temperature.

2.7. Analysis of the pH and point of zero charge (PZC)

The adsorption capacity of the MAGZA composite towards BOD, COD and TOC was investigated at pH 3 to 10. Overall, 2 mg/L of MAGZA composite was placed in a 200 mL conical flask containing 50 mL of the adsorbate solution at the initial concentration (20 mg/L) and investigated at the initial pH of 3, 4, 5, 6, 7, 8, 9 and 10 for 1 h. In the end, the solution was filtered using Whatman (No. 1) filter paper and the residual concentration of the BOD, COD and TOC was determined on the filtrate using the APHA standards [49]. Equally, the pH denoted as the point of zero charge (pH_{PZC}) of the MAGZA composite was evaluated by the associated titration method involving the mixing of 0.5 mg/L of adsorbent in deionized water. Subsequently, the adsorbent surface charge was regulated using NaOH and H_2SO_4 in the pH range of 2–12 until the attainment of a zero charge surface as reported elsewhere [56,57].

2.8. Column adsorption studies

For the column adsorption tests, a glass column of length (30 cm), internal diameter (3 cm) and volume (250 mL) was used. Eventually, MAGZA composite was selected for the adsorption studies at various bed heights (3, 4 and 5 cm), flow rates (4, 5 and 6 mL/min) and initial concentrations (10, 20 and 30 mg/L) based on the literature values and the preliminary experimentation. Particularly, 3 g of MAGZA was packed inside the glass column and supported by glass wool at both ends to prevent flow channelization and improve uniform dispersion of wastewater within the glass column. The effect of bed height, flow rate and initial concentration on the adsorptive removal of BOD, COD and TOC from textile wastewater was investigated by pumping the wastewater downwards from the tank to the column bed using a peristaltic pump as indicated in Fig. 1.

At intervals, glass conical flasks were used to collect effluent from the glass column and the residual concentrations of the BOD, COD and TOC were analyzed, calculated and recorded accordingly.

2.9. Mathematical description

Accordingly, the breakthrough curves which validate the industrial application of MAGZA were obtained by the plot of the normalized concentration which is depicted by the effluent to the influent concentration (C_t/C_o) versus time [32]. Particularly, the breakthrough time (t_b) and the shape of breakthrough curves have been identified as two primary features affecting the economics and feasibility of dynamic adsorption behaviour [56]. In that case, the nature of breakthrough curves and the associated parameters are dependent on the operating conditions of the fixed-bed column such as flow rate (Q), adsorbent bed height/depth (H) and inlet adsorbate concentration (C_o). The experimental evaluation of these parameters is important for the performance determination and scale-up of the column [58]. Generally, the time equivalence to useable capacity (breakthrough time, t_b) and the time equivalence to stoichiometric/total capacity (exhaustion time, t_e) are represented by Eqs. (1) and (2) [59].

$$t_b = \int_{t=0}^{t_b} \left(1 - \frac{C_t}{C_o}\right) dt \tag{1}$$

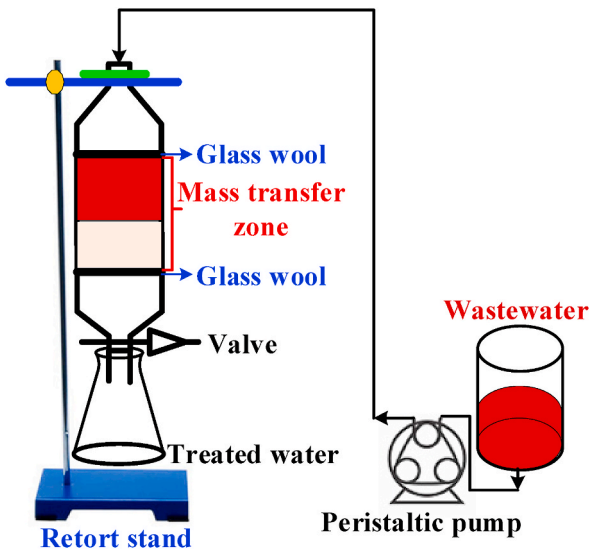

Fig. 1. Fixed-bed column representation of BOC, COD and TOC adsorption using MAGZA composite.

$$t_e = \int_{t=0}^{t=total} \left(1 - \frac{C_t}{C_o}\right) dt \quad (2)$$

where C_o and C_t are the inlet and outlet concentrations of BOD, COD and TOC in mg/L.

For the adsorption of BOD, COD and TOC in a fixed-bed column, the breakthrough time (t_b) designates the column condition where the concentration of BOD, COD and TOC in the effluent from the column attains or surpasses the 7, 40 and 6 mg/L permissible concentration limit (recommended by WHO/EPA). Conversely, the exhaustion time (t_e) is defined as the period in fixed-bed adsorption column when effluent concentration attains the 99% of adsorbate inlet concentration (C_t/C_o = 0.99) [56]. At t_e, the fixed-bed adsorption column is nearly exhausted. Consequently, the fixed-bed adsorption column was operated in this study until the achievement of the exhaustion time.

Importantly too, the total amount of adsorbed BOD, COD and TOC (q_{total}, mg) in the fixed-bed column at the specified concentration (C_t) and flow rate (Q) was calculated using Eq. (3) [60,61].

$$q_{total} = \frac{QA}{1000} = \frac{Q}{1000} \int_{t=0}^{t=t_{total}} (C_o - C_t) dt = \frac{(C_0 - C_t) Q t_e}{1000} = (C_0 - C_t) V_e \quad (3)$$

where A and C_o - C_t (mg/L) represent the area under the breakthrough curve and the adsorbed quantities of BOD, COD and TOC, respectively. The parameters such as t_e and V_e in min and L depict the MAGZA composite bed saturation time and the collected total volume of effluent until the point of saturation. The initial concentrations of BOD, COD and TOC were denoted by C_o (mg/L), while C_t (mg/L) and V_e show the concentrations and volume of the effluent, respectively.

The equilibrium adsorption capacity (q_{eq}, mg/g) of BOD, COD and TOC at the point of exhaustion per unit dry weight of MAGZA added to the bed column was determined by Eq. (4) [62].

$$q_{eq} = \frac{q_{total}}{m} \quad (4)$$

in which m (g) refer to the total amount of MAGZA packed inside the glass column.

Furthermore, the evaluation of the percentage removal of BOD, COD and TOC (R%) at the bed column point of exhaustion and the total amount of BOD, COD and TOC passed through the MAGZA bed column until the point of exhaustion was determined by Eqs. (5) and (6) [63], respectively.

$$R\% = \frac{q_{total}}{m_{total}} \text{ x } 100 \quad (5)$$

$$m_{total} = \frac{C_o Q t_{total}}{1000} = \frac{C_o \text{ x } Q \text{ x } t_e}{1000} = C_o \text{ x } V_e \quad (6)$$

Meanwhile, the length of the mass transfer zone (L_{MTZ}) which is the length of the adsorption zone representing the adsorbent efficiency in the fixed bed was estimated by Eq. (7) [3].

$$L_{MTZ} = H\left(\frac{t_e - t_b}{t_e}\right) \quad (7)$$

The empty bed contact time (EBCT) is the contact time between the adsorbate solution and the adsorbent in the fixed-bed column. The value of EBCT was evaluated by the mathematical representation in Eq. (8) [64].

$$EBCT = \frac{V}{Q} \quad (8)$$

The volume of effluent (V_{eff}) or the volume of the treated adsorbate solution was determined by Eq. (9) [65].

$$V_{eff} = Q t_e \quad (9)$$

in which, V (L), H (cm) and Q (mL/min) refer to the adsorbate volume, adsorbent bed height and flow rate, respectively.

2.10. Regeneration and reusability

Sequel to the reduction of cost and environmental protection from the deposition of solid waste, adsorbent desorption and recycling have gathered momentum. Before now, NaOH solution has been reported as a good desorption reagent due to its free hydroxyl ions (OH^-) [56]. For this purpose, NaOH was utilized for the regeneration of the adsorbent and a maximum percentage regeneration of spent MAGZA composite was obtained at 2.5 M of NaOH (Fig. S3, Supplementary material). Therefore, the regeneration and reusability of the spent MAGZA composite in a fixed-bed column were conducted using 2.5 M NaOH at a flow rate (4 mL/min), bed depth (5 cm), inlet concentrations of BOD, COD and TOC (10 mg/L) and pH (6.5). To achieve the regeneration operation, NaOH solution (2.5 M) was introduced into the exhausted adsorbent bed in the column at the flow rate of 4 mL/min until the effluent concentration

showed a negligible amount of BOD, COD and TOC. Further study of the reusability was conducted by the passage of distilled water through the adsorbent bed column for the removal of the excess quantity of NaOH from the adsorbent until a significant decline of the effluent alkalinity was observed. Also, a dilute H_2SO_4 (0.1 M) was introduced into the adsorbent bed column at the flow rate of 4 mL/min to reduce the alkalinity of the adsorbent caused by NaOH traces until the effluent showed a pH of around 7.5. Again, distilled water was passed through the adsorbent bed column for the removal of remaining NaOH from the adsorbent sample at the flow rate (4 mL/min) until the effluent pH was close to 7. At the end of this step, the next adsorption cycle (reusability cycle) was conducted repeatedly until a significant reduction in t_b and t_e was achieved.

3. Results and discussion

3.1. Characterization of materials

Herein, the addition of MIL extract to the iron salt solution enabled the change of the brown colour of the MIL extract to dark red which indicated the formation of magnetite NPs (Fe_3O_4 NPs). During the formation period of magnetite NPs, the pH decreased which suggested the contribution of hydroxyl (OH) groups in the reduction of iron sulphate solution to ferrous and ferric hydroxide through the liberation of H^+ ions [1]. In this study, phytochemicals such as flavonoids, amino acids, polyphenols, terpenoids and saponins present in MIL extract are used as a reactant to nucleate the NPs in the reacting mixture [66]. The colour change of the reacting mixture was used for the visual fabrication confirmation. Thus, the reacting mixture change in colour may be ascribed to the phenomenon of surface plasmon resonance (SPR) in the magnetite NPs. The influence of SPR combines the oscillation conduction band electrons (OCBE) of metal NPs whereby the incident photons frequency matches that of metal NPs OCBE [67]. Particularly, the phenomenon occurs when the particle size attains the nanoscale range. To confirm and authenticate the fabrication and stability of NPs, UV–Vis

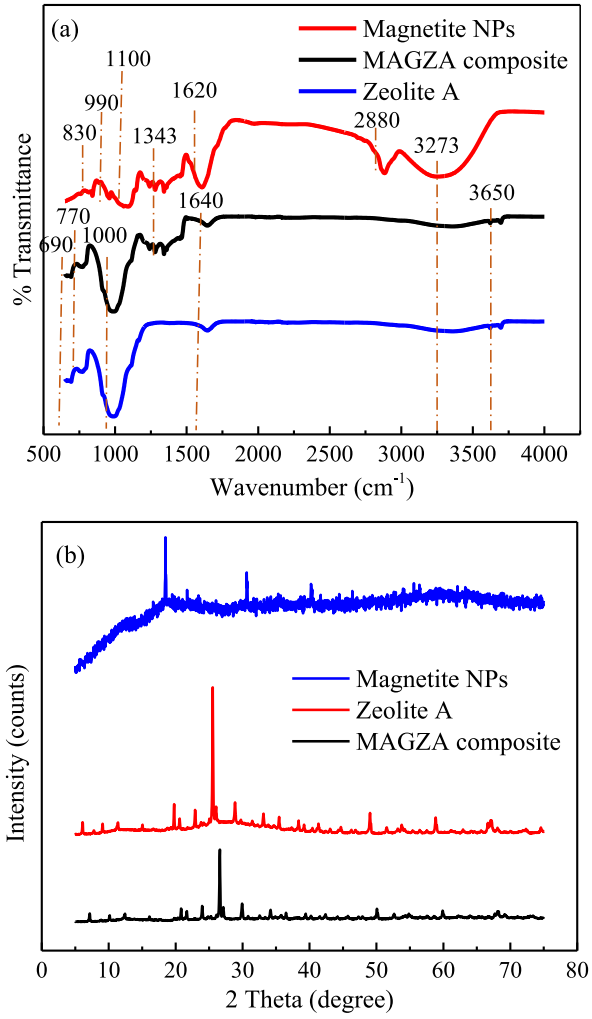

Fig. 2. (a) FTIR and (b) XRD of Magnetite NPs, Zeolite A and MAGZA composite.

absorption spectroscopy is predominantly utilized due to the sensitivity of SPR absorbance wavelength and shape towards the particle size, morphology, agglomeration, metallic dielectric functions and the environment [66]. The MIL extract shows a specific peak at 280 nm which relates to the presence of polyphenolic compounds [68]. After the synthesis period, the maximum absorption peak monitored by UV–Vis spectroscopy was reduced to 259 nm as shown in Fig. S1 (Supplementary Information), due to the formation of magnetite NPs of smaller particle size.

FTIR analysis was conducted to evaluate the functional group of magnetite NPs, zeolite A and MAGZA composite. According to Sazali et al. [69], Al–O bending mode were described at 752 cm^{-1} and 800 cm^{-1}, while Si–O stretching vibrations were identified at 700 cm^{-1} and 1033 cm^{-1}. From Fig. 2(a), the absorption band at 690 cm^{-1} may be associated with the Si–*O*-T symmetric stretching vibrations of the sodalite framework for hydrosodalite zeolite and showed appreciable correspondence with the literature [69,70]. As seen from the spectra of zeolite A and MAGZA composite, the vibration peak that occurred at 770 cm^{-1} may be ascribed to the Al–O and Si–O bending mode of metakaolin [69,71]. The band at 830 cm^{-1} on the magnetite NPs belongs to the Fe–O group, while the vibrational peaks at 990 and 1100 cm^{-1} represent the C–H and C–O bending vibration modes [1,72]. The band at 1000 cm^{-1} that occurred on zeolite A and MAGZA composite was assigned to the asymmetric stretching vibrations of all zeolite materials such as Si–O and Al–O that may be attributed to tetrahedron bond frequencies of (Si, Al)–O along the connecting lines of [(Si, Al)O_4] 4-tetrahedron oxygen atoms with Si/Al central atoms [42,69,70]. Specifically, the characteristic peak at 1343 cm^{-1} substantiated the presence of iron corresponding to the formation of magnetite, hematite and lepidocrocite on the surfaces of Fe^0 and the MAGZA composite surfaces [42]. Also on the magnetite NPs, the spectrum at 1620 cm^{-1} may be attributed to the occurrence of polyphenol aromatic rings and N–H bonds formed during the reduction of Fe^{+2} and Fe^{+3} salts by the addition of mango leaves extract [72,73]. Specifically, on the zeolite A and MAGZA composite, the band observed at 1640 may be assigned to O–H bending vibration of water molecules [42]. The band at 2880 cm^{-1} on the magnetite NPs may be attributed to the –COOH stretch [74], while the broad peak at 3273 cm^{-1} indicates O–H stretching vibrations on the magnetite NPs, zeolite A and MAGZA composite [1]. In addition, the band occurrence at 3650 cm^{-1} with a

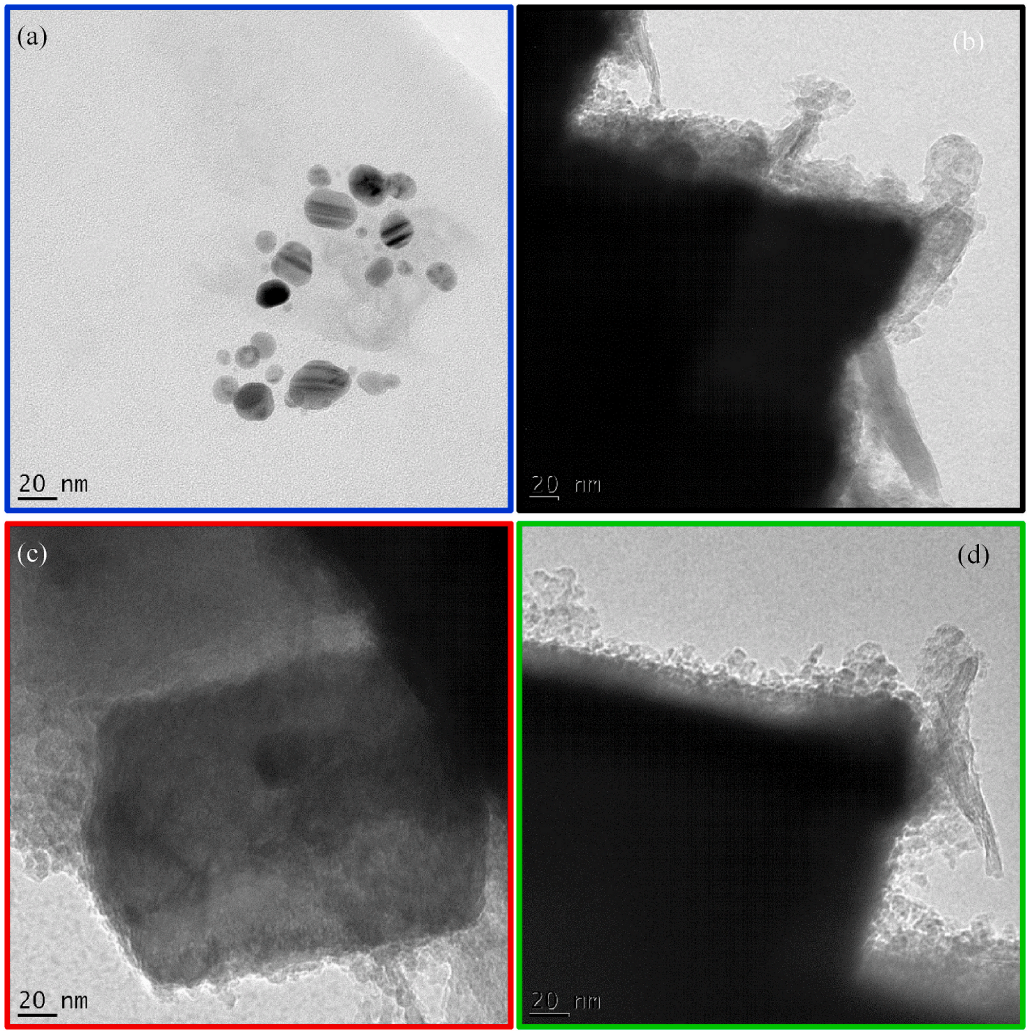

Fig. 3. TEM Micrograph of (a) Magnetite NPs; (b) Zeolite A; MAGZA composite (c) before adsorption and (d) after adsorption.

small peak observed on the zeolite A and MAGZA composite samples may be assigned to the O–H dissociation [42]. Furthermore, the occurrence of FeO on the SiO_4 and AlO_4 surface matrix of MAGZA composite caused the rupture of hydrogen bonds, weakening of intensities and shifting of bands at 1100 cm^{-1}, 1620 cm^{-1} and 3273 cm^{-1} [42,46] Therefore, the FTIR study confirmed successful incorporation of magnetite on the surface framework of zeolite material and further supported the XRD which showed a reduction in the intensities of the peaks of the composite compared to the magnetite and the zeolite A samples.

The crystalline patterns of magnetite nanoparticles, zeolite A and MAGZA composite were investigated as shown in Fig. 2(b). According to Fig. 2(b), the diffraction peak presence at 2θ around the 18.48° (002) plane may be linked to the amorphous nature of magnetite NPs crystal structure which may be attributed to green synthesis [1,74]. Particularly, the characteristic peaks of Fe_3O_4 nanoparticles were evident at 2θ values of 30.62°, 40.19°, 45.70°, 52.35°, 57.10° and 62.11°, respectively which corresponded with the diffraction patterns of magnetite (JCPS card no: 00-033-0664) [42,46,75]. The XRD patterns of zeolite A in Fig. 2(b) revealed the occurrence of intense diffraction peaks at 2θ values of 7.10°, 10.10°, 16.02°, 21.64°, 24.00°, 29.92°, 30.07° and 32.52° which may be due to the SiO2 crystalline peaks on the zeolite [45,75]. On the other hand, the appearance of peaks at 12.40°, 26.55°, 34.06°, 36.43°, 50.00°, 59.81°, 62.32° and 68.26° indicated the detection of the presence of Al_2O_3 on the zeolite A [46]. In the case of the MAGZA composite, the presence of characteristic diffraction patterns corresponding to magnetite NPs and zeolite A confirmed the successful incorporation of magnetite NPs into the framework of the zeolite A structure. However, the observed decrease in the peak intensity of MAGZA composite could be attributable to the hybrid formation, suggesting that mango leaves extract and the magnetite NPs acted as a capping agent and stabilizer on the coverage of zeolite A surface, thus roughening the characteristic peaks of zeolite A [45,46].

The microstructure of magnetite NPs, zeolite A and MAGZA composite are shown in Fig. 3(a,b,c). The result in Fig. 3(a) revealed well-dispersed spherical magnetite NPs with an average particle size of 10.17 nm. As shown in Fig. 3(b), the typical cubic shape of zeolite A was evident with a smooth surface [75]. The TEM analysis of the magnetite NPs doped zeolite A was also performed to investigate the changes in the morphology of zeolite A after doping with magnetite as shown in Fig. 3(c).

Accordingly, the incorporated magnetite NPs appeared to be evenly dispersed on the surface, edges and porous spaces of the zeolite A indicated by the black spherical patches which may be attributed to the presence of numerous magnetite NPs that got embedded in the zeolite network [45,46]. Noticeably, the magnetite NPs are clustered on the surface of zeolite A possibly due to the crystalline nature of the magnetite NPs that agglomerate the particles as a result of attraction between the particles and the zeolite A [76]. Similarly, a marked change in the microstructure of zeolite A after the incorporation of magnetite NPs was evident with the presence of a rough surface having cracks and macropores due to the replacement of amorphous Al/Si from the matrix during sodium hydroxide solution added to the suspension of zeolite [75]. The surface roughness of the zeolite A particle enhances the deposition of the magnetite NPs in smaller aggregates for overall coverage of the exposed surfaces of the zeolite by the magnetite NPs. In comparison to the discrete magnetite NPs and zeolite A, the fabricated hybrid MAGZA composite was dispersive to enable improved removal of BOD, COD and TOC from wastewater. Further investigation of the microstructure of the MAGZA composite after adsorption studies was conducted and shown in Fig. 3(d). The EDX results of the zeolite A and the MAGZA composite showing the successful preparation of the composite are shown in Figs. S2 and S3. Overall, the cubic structure did not indicate noticeable change, but aggregation into bulks of irregularly shaped particles was observed with whitish deposits on the edges of the composite that may be linked to the adsorbed BOD, COD and TOC pollutants.

Further investigation of the surface properties and particle size distribution of magnetite NPs, zeolite A and MAGZA composite was conducted and presented in Table 1.

As can be seen in Table 1, all the particles of magnetite NPs were in the nanometer range (<100 nm) with a surface area of 95.26 ± 2 m^2/g. The zeolite A had a surface area of 119.98 ± 3 m^2/g with the particle size predominantly in the range of 2 and 20 μm (56.6 ± 0.1%). For the MAGZA composite, the BET surface area was recorded as 110.50 ± 6 m^2/g with the major percentage of particle size between 20 and 50 μm range (75.2 ± 0.2%). Overall, the observed decrease in the surface area and increase in the particle size may be attributed to the iron oxide NPs doping during the fabrication of the composite [76]. Doping enhances the agglomeration of particles by blocking the abundant porous network of zeolite A through cementation, thereby reducing the surface area of the composite material.

Table 1
Surface properties and particle size distribution for magnetite NPs, zeolite A and magnetite-zeolite A composite.

Parameters	Magnetite NPs	Zeolite A	MAGZA composite
BET surface area (m^2/g)	95.26 ± 2	119.98 ± 3	110.50 ± 6
Pore diameter (nm)	2.54 ± 0.04	3.328 ± 0.3	6.32 ± 0.8
Total pore volume (g/cm^3)	0.028 ± 0.1	0.039 ± 0.1	0.185 ± 0.2
Particcle size (nm)			
<2 (nm)[a]	–	18.2 ± 0.1	6.8 ± 0.2
2–20 (nm)[a]	–	56.6 ± 0.1	16.5 ± 0.1
20–50 (nm)[a]	–	20.8 ± 0.1	75.2 ± 0.2
>50 (nm)[a]	–	4.4 ± 0.1	1.5 ± 0.2
<100 (nm)[b]	100	–	–

[a] Evaluated by the pipette technique and.
[b] Evaluated by TEM analysis.

3.2. Selectivity of adsorbents

Herein, the prepared adsorbents (magnetite NPs, zeolite A and MAGZA composite) were applied for the adsorption of BOD, COD and TOC from textile wastewater as indicated in Fig. 4(a,b,c).

As can be seen from the result, the fixed-bed adsorption of the BOD, COD and TOC was relatively higher using MAGZA composite,

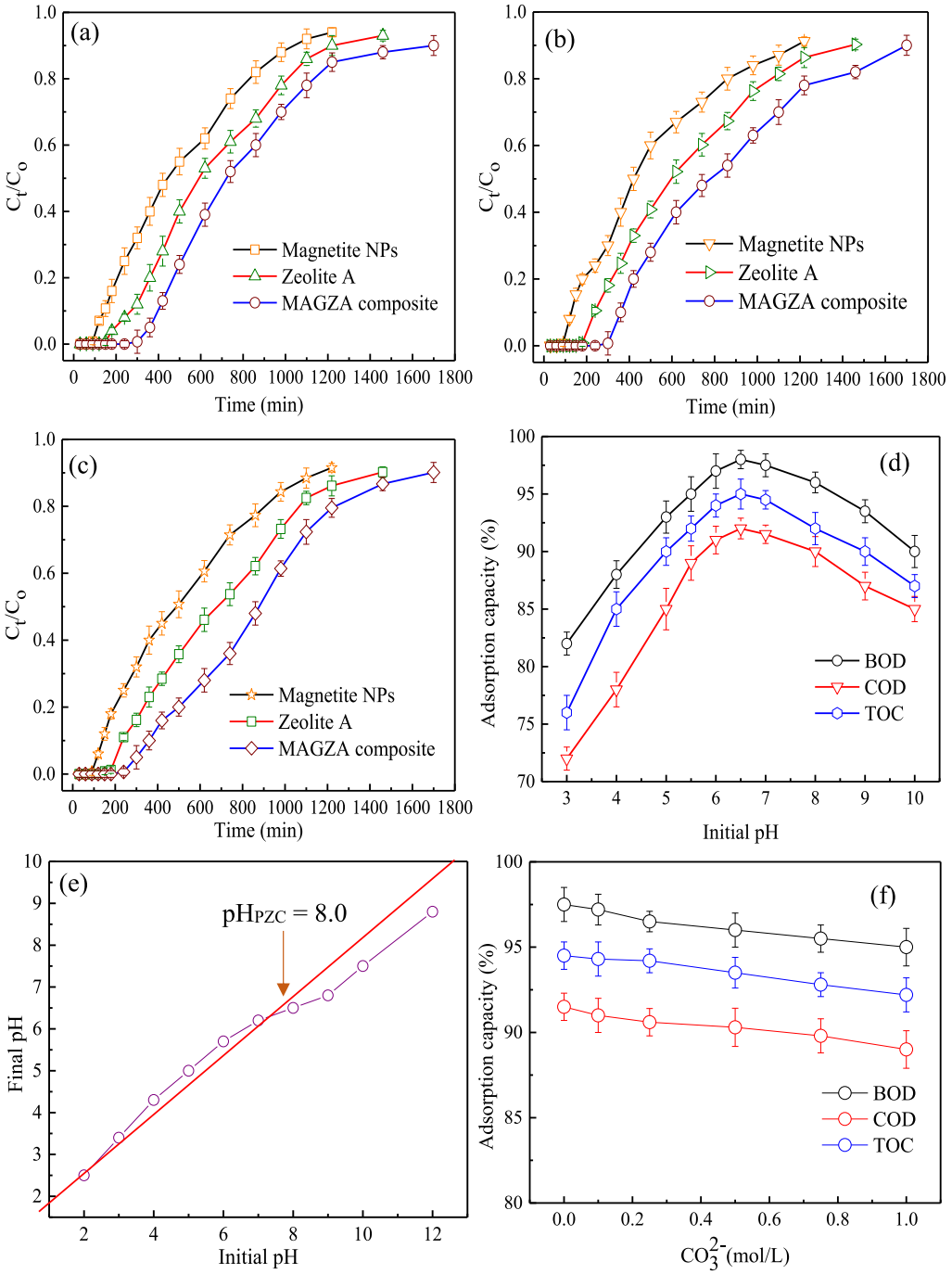

Fig. 4. (a) Comparative adsorption performance of magnetite NPs, zeolite A and MAGZA composite towards (a) BOD; (b) COD; (c) TOC; (d) Equilibrium BOD, COD and TOC percentage adsorption by MAGZA adsorbent at different pH at adsorbate concentration (20 mg/L), adsorbent dose (10 mg/L), contact time (60 min), stirring speed (200 rpm) and temperature (25 °C); (e) pH_{PZC} of MAGZA composite adsorbent and (f) the effect of coexisting carbonate ions on the adsorption process (pH 6.5, adsorbent amount (2 mg/L), initial concentration (20 mg/L) and temperature (25 °C).

followed by zeolite A and then magnetite NPs. For instance, the breakthrough time and exhaustion time were longer in the MAGZA composite, followed by zeolite A and then magnetite NPs that were closer to the origin. For the adsorption of BOD and COD, the breakthrough time was obtained as 150, 240 and 360 min using magnetite NPs, zeolite A and MAGZA composite, while the exhaustion time was recorded as 1220, 1460 and 1700 min, respectively. On the other hand, the breakthrough time of 150, 300, 420 min and exhaustion times of 1100, 1220 and 1700 min were reported using magnetite NPs, zeolite A and MAGZA composite. In addition, the adsorption capacity of magnetite NPs, zeolite A and MAGZA composite by the Thomas model were also compared and the determined parameters are presented in Table 2.

It is evident in Table 2 that the adsorption capacity (q_o) of BOD, COD and TOC were obtained as 255.98, 241.94 and 243.36 mg/g for magnetite NPs, while the adsorption capacities of 323.66, 295.79 and 302.92 mg/g were attained for BOD, COD and TOC using zeolite A. Also, the adsorption capacity of 385.86, 330.10 and 374.01 mg/g were reported for the BOD, COD and TOC using MAGZA composite. Similarly, the statistical data from correlation coefficient (R^2) and Chi-square (X^2) revealed higher R^2 values and lower X^2 values for MAGZA composite towards the removal of BOD, COD and TOC. The observed higher adsorption efficiency of MAGZA composite compared to zeolite A and magnetite NPs may be attributed to higher adsorption sites present on the adsorbent surface due to the incorporation of magnetite NPs on the surface matrix of zeolite A. Similar reports on improved adsorption efficiency have been reported elsewhere [8,77]. Sequel to the higher adsorption capacity indicated by the MAGZA composite, the composite was selected for further adsorption studies in the treatment of textile wastewater.

3.3. Effect of solution pH

Generally, wastewater from textile industries contains organic pollutants, chemical substances, carbonaceous pollutants, nitrogen, sulphur, fluoride, chloride and phosphorous pollutants that are toxic to the environment and human health. As such, pH is a significant parameter affecting the adsorptive removal of pollutants by the adsorbents due to the profound influence of adsorption sites on the surface of the adsorbent. Overall, the sign and degree of the surface charge on the adsorbent primarily depend on the solution pH. Therefore, the effect of pH on the adsorption of BOD, COD and TOC by MAGZA composite was investigated in the pH range of 3–12 as shown in Fig. 4(d). As can be seen in Fig. 4(d), the adsorption of BOD increased gradually from pH 3 to the optimal pH of 6.5 beyond which a significant decline was observed. A similar increment in the percentage adsorption was recorded for both COD and TOC. The optimum adsorption of 98, 92 and 95% were obtained for BOD, COD and TOC at a pH of 6.5. Therefore, the maximum adsorption of BOD, COD and TOC was achieved at pH 6.5. The observed trend in this study may be attributed to the acidity/alkalinity and surface charge of the MAGZA composite. The adsorption of BOD, COD and TOC at lower pH was noticeably low, perhaps due to the positive surface charge of the MAGZA composite. This may be attributed to the hindrance associated with H^+ ions between the BOD/COD/TOC molecules and the MAGZA composite binding sites.

Further investigation of the pH effect was explored by pH_{PZC} which was obtained as 6.5 (Fig. 4(e)). Accordingly, the surface of the MAGZA composite adsorbent is positively charged at $pH < pH_{PZC}$ and negatively charged at $pH > pH_{PZC}$. At pH 6.5, the electrostatic interaction between the adsorbents binding sites and the BOD/COD/TOC molecules was high, thereby leading to the observed optimum adsorption rate. At the pH of 7, the adsorption rate declined which may be attributed to the competition between the BOD/COD/TOC molecules and hydroxyl (OH^-) group for the adsorption sites on the MAGZA composite [77]. Beyond the pH 8, further reduction in the percentage of adsorption was evident due to the increasing electrostatic repulsion between the negatively charged surface of the adsorbent and the BOD/COD/TOC molecules. Over the literature, similar findings have been reported previously [78].

The influence of carbonate ions (CO_3^{2-}) were investigated on the textile wastewater towards the removal of BOD, COD and TOC by MAGZA composite at pH (6.5), adsorbent amount (2 mg/L), initial concentration (20 mg/L) and temperature (25 °C). Carbonate ions exist in an electronegative form that creates a competitive environment for the adsorption of BOD, COD and TOC in the MAGZA bed column. The resultant influence of the presence of carbonate ions is evident in Fig. 4(f). Noticeably, a reduction in the removal of BOD, COD and TOC was observed as the concentration of carbonate ions increased. Above all, at the higher CO_3^{2-} concentration of 1 mol/L, the adsorption capacity of BOD, COD and TOC declined to 95, 89 and 92.2%, respectively from 97.5, 91.5 and 94.5% without the competing ions. Therefore, the result revealed moderate competition or hindrance towards the adsorption of BOD, COD and TOC by MAGZA composite. The result of this study showed a similar trend reported in the literature [56].

Table 2
Comparison of adsorption capacity of magnetite NPs, zeolite A and MAGZA composite by Thomas model (operating conditions: flow rate (4 mL/min), bed height (4 cm) and inlet concentration (20 mg/L)).

Adsorbate	Adsorbent	k_{TH}	q_o	R^2	X^2
BOD	Magnetite NPs	0.0052	255.88	0.968	0.0038
	Zeolite A	0.0049	323.66	0.977	0.0029
	MAGZA composite	0.0049	385.86	0.989	0.0023
COD	Magnetite NPs	0.0050	241.94	0.953	0.0052
	Zeolite A	0.0045	295.79	0.961	0.0045
	MAGZA composite	0.0039	330.10	0.985	0.0040
TOC	Magnetite NPs	0.0046	243.36	0.958	0.0044
	Zeolite A	0.0043	302.92	0.972	0.0034
	MAGZA composite	0.0042	374.01	0.987	0.0031

3.4. Effect of operating parameters on the adsorption of BOD, COD and TOC

The effect of parameters such as flow rate (Q, mL/min), bed height (H, cm) and inlet adsorbate concentration (C_o, mg/L) on the adsorption of BOD, COD and TOC by MAGZA composite as adsorbent was investigated in a continuous fixed-bed column. The detailed explanation of these parameters in a dynamic operation of the bed column is evaluated.

3.4.1. The effect of adsorbate flow rate on the breakthrough curve

The effect of flow rate on the removal of BOD, COD and TOC by MAGZA composite was investigated at 4, 5 and 6 mL/min at constant bed height (5 cm), inlet adsorbate concentration (10 mg/L), solution pH (6.5) and temperature (25 °C). The results shown in Fig. 5(a,b,c) illustrated the nature of the breakthrough curves on the variation of the different flow rates which noticeably indicated that a lower flow rate of 4 mL/min provided abundant contact time for the mass transfer of adsorbate to the pores on the surface of MAGZA composite. As can be seen in Fig. 5(a,b,c), an increase in the flow rate of the adsorbate (BOD, COD and TOC) from 4 to 6 mL/min quickened the attainment of the breakthrough point, thus reducing the t_b from 360 to 120 min for BOD, 300 to 150 min for COD, 420 to 120 min for TOC and t_e from 1740 to 1020 min for BOD, 1700 to 1100 min for COD and 1680 to 1020 min for TOC. The changes in the breakthrough curves may be linked to the fast mass transfer of BOD, COD and TOC to the bulk surface, thereby rapidly occupying the active sites of the MAGZA composite. It is evident that the rate of mass transfer is improved at a high flow rate which enhanced the amount of BOD, COD and TOC adsorbed by the adsorbent, thus rapidly facilitating the saturation of the column bed at a high flow rate.

At a higher flow rate, lower contact time and higher turbulence were observed which resulted in weak interaction of the adsorbent-adsorbate and a reduction in the distribution of intraparticle transfer of mass between the molecules of the adsorbate and the composite. The insufficient contact time of the BOD, COD, TOC and MAGZA composite resulted in a reduction in the adsorption of the

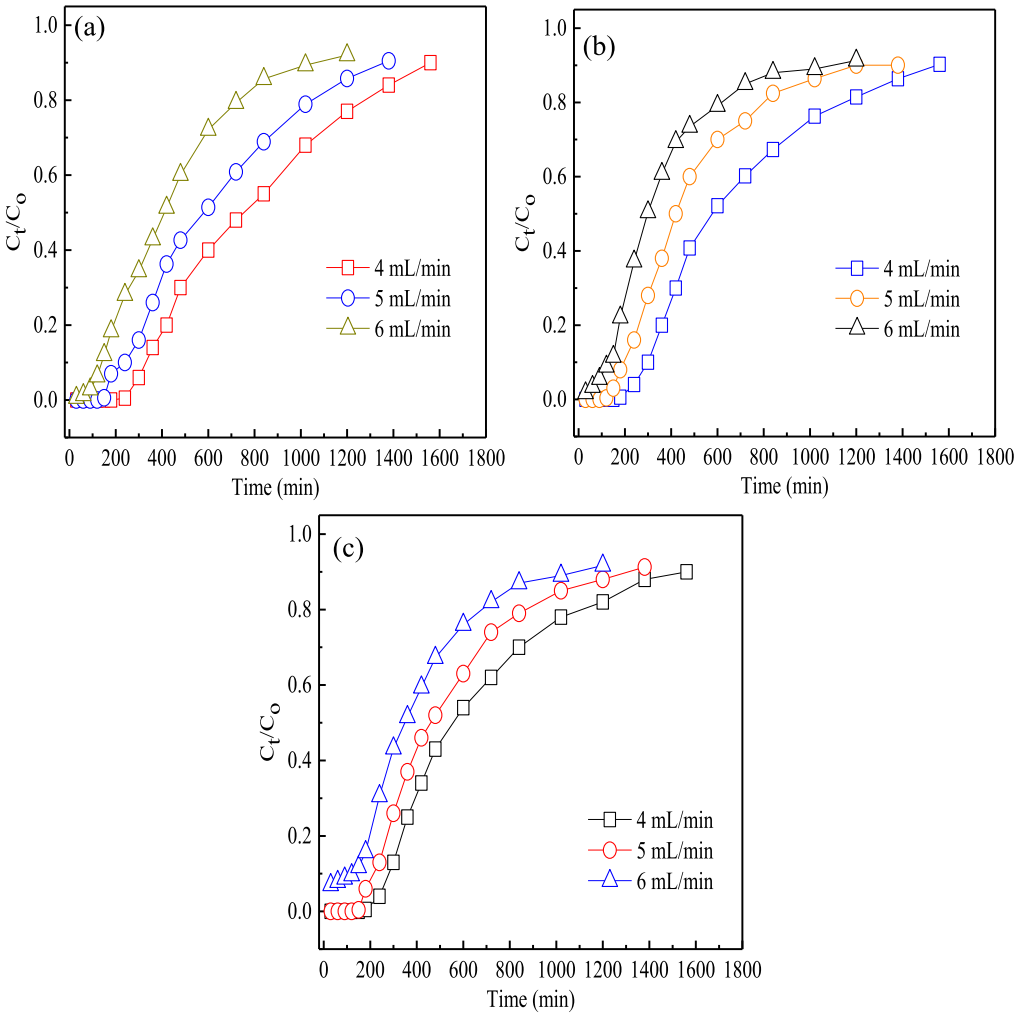

Fig. 5. The effect of flow rate on the breakthrough curve for the removal of (a) BOD; (b) COD and (c) TOC from the textile effluent at pH = 6.5 and temperature = 25 °C.

organic pollutants. Overall, an increase in the flow rate of the adsorbate reduces the external mass transfer film thickness and the accompanied resistance, thereby increasing the mass transfer coefficient and flux [56]. Although the mass transfer zone (MTZ) is widened by an increase in the adsorbate flow rate, the used fractional bed is narrowed.

As presented in Table 3, the adsorption capacity decreased from 67.42 to 50.49 mg/g for BOD, 66.10 to 54.45 mg/g for COD and 60.44 to 46.53 mg/g for TOC as the adsorbate flow rate increased from 4 to 6 mL/min. Additionally, the empty bed contact time (EBCT) was also reduced from 1.74 to 1.02 min for BOD, 1.70 to 1.10 min for COD and 1.68 to 0.94 min for TOC with an increasing flow rate from 4 to 6 mL/min. The trend of this result indicates that a larger amount of BOD, COD and TOC are leaving the bed column without being captured before attaining adsorption equilibrium due to insufficient contact between the adsorbate and adsorbent at a higher flow rate. Other researchers noticed similar observations too [79,80]. On the other hand, the decrease in the adsorption capacity is an indication that the lower flow rate was favourable, thereby increasing the adsorption capacity due to the larger contact time for the interaction of adsorbent-adsorbate and extended intraparticle diffusion of the adsorbate onto the adsorbent surface [56,60,81].

3.4.2. The effect of composite bed heights on the breakthrough curve

Bed height is a major parameter in the evaluation of breakthrough curves performance of fixed-bed column and it is directly proportional to the adsorbent amount. As such, Fig. 6(a,b,c) demonstrates the breakthrough curves of BOD, COD and TOC adsorption at the bed depths of 3, 4 and 5 cm, respectively, while maintaining other parameters such as inlet concentration, flow rate, solution pH and temperature at a constant value of 10 mg/L, 4 mL/min, 6.5 and 25 °C.

Specifically, the trends of results in Fig. 6(a,b,c) revealed that the breakthrough time and exhaustion time were increased as the bed depth was increased. For instance, the breakthrough time and exhaustion time of BOD, COD and TOC increased from 90 to 420 and 1260–1740 min as the bed height increased from 3 to 5 cm. Furthermore, the slope of the breakthrough curve decreased, while an enhanced mass transfer zone was developed as shown in Table 3. A similar trend in this study was also reported by Refs. [3,32,82]. The observed increase may be attributed to the higher adsorbent mass that provided larger active sites for the adsorption of BOD, COD and TOC. In addition, the improvement in bed height increased the length of empty bed contact time, thereby increasing the contact time for the adsorbent and the adsorbate to interact. Meanwhile, smaller bed depths are saturated quickly compared to larger bed depths due to the availability of less active surfaces for adsorption and a shorter time for the BOD/COD/TOC and MAGZA composite contact. Above all, the dynamic adsorption data and parameters obtained from the influence of bed height on the uptake of BOD, COD and TOC using MAGZA composite are presented in Table 3. According to Table 3, an increase in bed height from 3 to 5 cm resulted in an increase in the effluent volume, adsorbed amount, length of mass transfer, adsorption capacity, adsorption efficiency and the EBCT. Particularly, the adsorption capacity of the organic pollutants increased from 45.54 to 67.52 mg/g for BOD, 43.56–66.10 mg/g for COD and 41.58–60.44 mg/g for TOC, respectively. This indicates that the bed height of the adsorbent strongly affects the adsorption of BOD, COD and TOC in the column and similar observations have been reported by other researchers [3,56,58].

3.4.3. The effect of adsorbate inlet concentration on the breakthrough curve

In this study, the effect of BOD, COD and TOC concentration on the column performance and breakthrough curve was conducted in the range of 10–30 mg/L at constant bed height (5 cm), flow rate (4 mL/min), solution pH (6.5) and temperature (25 °C). As can be seen in Fig. 7(a,b,c), the breakthrough curve was observed to be steep and shifted towards the origin as the adsorbate inlet

Table 3
Dynamic column parameters of breakthrough curve for the adsorption of BOD, COD and TOC by MAGZA composite.

Adsorbate	Q	H	C_o	t_b	t_e	V_{eff}	q_{total}	L_{MTZ}	q_e	m_{total}	R	EBCT
	(mL/min)	(cm)	(mg/L)	(min)	(min)	(L)	(mg)	(cm)	(mg/g)	(mg)	(%)	(min)
BOD	4	3	10	90	1380	5.52	54.65	2.80	45.54	55.20	99.85	1.38
	4	4	10	240	1620	6.48	64.15	3.41	53.46	64.80	99.90	1.62
	4	5	10	360	1740	6.96	68.90	3.97	67.42	69.60	99.96	1.74
	4	5	20	240	1640	6.56	130.54	4.27	108.79	131.20	99.68	1.64
	4	5	30	160	1560	6.24	186.58	4.49	155.48	187.20	99.75	1.56
	5	5	10	240	1460	7.30	72.27	4.18	60.23	73.00	99.70	1.46
	6	5	10	120	1020	6.12	60.59	4.01	50.49	61.20	99.56	1.02
COD	4	3	10	180	1320	5.28	52.27	2.59	43.56	52.80	99.70	1.32
	4	4	10	240	1560	6.24	61.78	3.38	51.48	62.40	99.80	1.56
	4	5	10	300	1700	6.80	67.32	4.12	66.10	68.00	99.88	1.70
	4	5	20	180	1200	4.80	95.52	4.25	79.60	96.00	99.68	1.20
	4	5	30	120	1020	4.08	121.99	4.41	101.66	122.40	99.60	1.02
	5	5	10	240	1440	7.20	71.28	4.17	59.40	72.00	99.55	1.44
	6	5	10	150	1100	6.60	65.34	4.02	54.45	66.00	99.20	1.10
TOC	4	3	10	150	1260	5.04	49.90	2.64	41.58	50.40	99.65	1.26
	4	4	10	240	1500	6.00	59.40	3.36	49.50	60.00	99.73	1.50
	4	5	10	420	1680	6.72	66.53	3.75	60.44	67.20	99.87	1.68
	4	5	20	240	1380	5.52	109.85	4.13	91.54	110.40	99.67	1.38
	4	5	30	150	1200	4.80	143.52	4.38	119.60	144.00	99.50	1.20
	5	5	10	240	1380	6.90	68.31	4.13	56.93	69.00	99.25	1.38
	6	5	10	120	1020	5.64	55.84	4.06	46.53	56.40	99.00	0.94

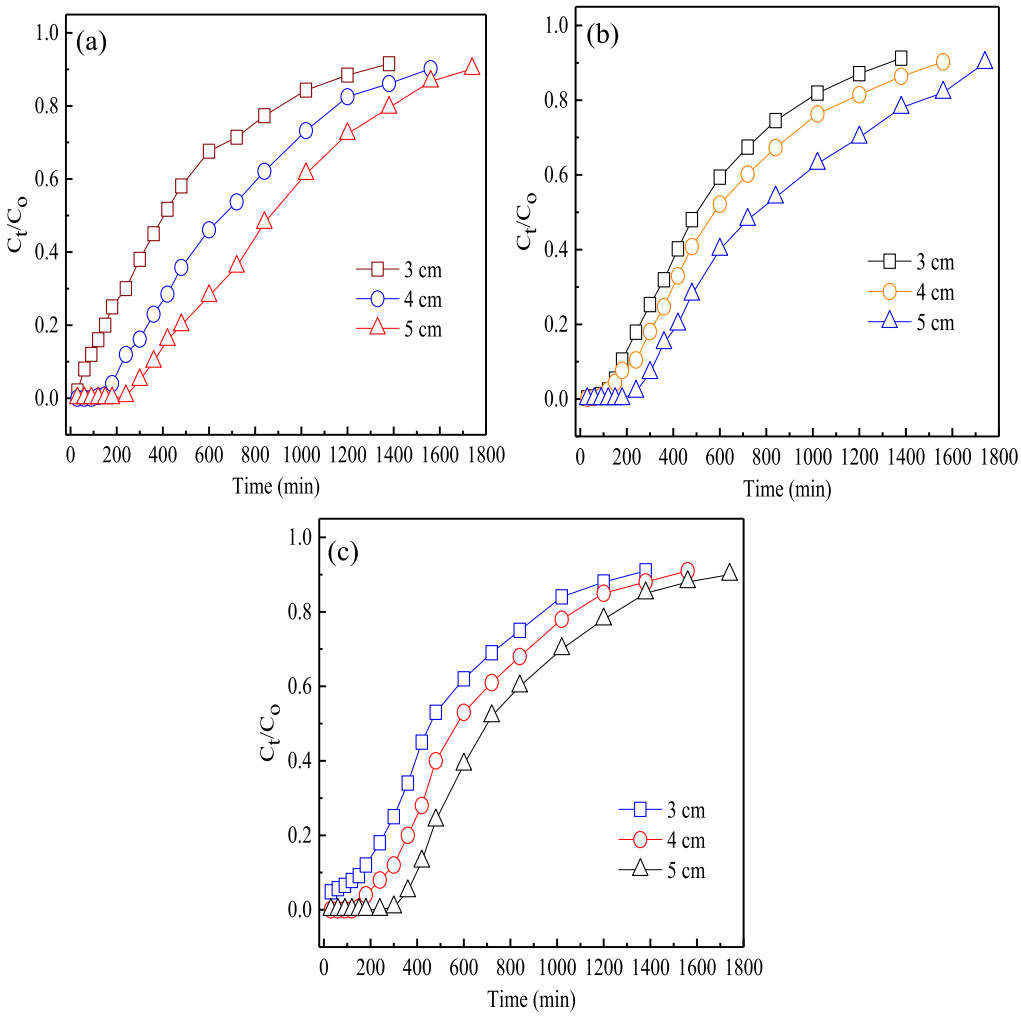

Fig. 6. The effect of bed height on the breakthrough curve for the removal of (a) BOD; (b) COD and (c) TOC from the textile effluent at pH = 6.5 and temperature = 25 °C.

concentration increased from 10 to 30 mg/L. This trend may be ascribed to the strong driving force observed from higher concentration gradient emanating from higher concentrations of BOD, COD and TOC. As such, the fast attainment of the breakthrough time and exhaustion time may be attributable to the increased diffusion of adsorbed molecules which enhanced the completion of the adsorption cycle at a reduced time [77]. However, at lower adsorbate inlet concentrations that produced a lower concentration gradient, slower transport was observed due to a decline in the mass transfer coefficient and diffusion coefficient [80,83].

As shown in Table 3, the increase in the organic pollutant inlet concentration (10, 20 and 30 mg/L) caused the observed decline in the breakthrough time (t_b) from 360 to 160 min for BOD, 300 to 120 min for COD, 420 to 150 min for TOC and the exhaustion time (t_e) from 1740 to 1560 min for BOD, 1700 to 1020 min for COD and 1680 to 1200 min for TOC, respectively. Similarly, the EBCT declined from 1.74 to 1.56 min for BOD, 1.70 to 1.02 min for COD and 1.68 to 1.20 min for TOC with an increase in adsorbate inlet concentration from 10 to 30 mg/L. Also, the removal efficiency of the adsorbate was observed to decrease from 99.96 to 99.75% for BOD, 99.88 to 99.60% for COD and 99.87 to 99.50% for TOC. The trend of this result may be ascribed to the rapid saturation of the active sites of the adsorbent at a higher amount of inlet adsorbate concentration which was also supported by other researchers [56,80]. However, the length of the mass transfer zone increased from 3.97 to 4.49 cm for BOD, 4.12–4.41 cm for COD and 3.75–4.38 cm for TOC, while the adsorption capacity also increased from 67.42 to 155.48 mg/g for BOD, 66.10–101.66 mg/g for COD and 60.44–119.60 mg/g for TOC, respectively. Above all, this observation may be ascribed to the enlarged driving force from the higher adsorbate inlet concentration gradient to overpower the mass transfer resistance [82,84].

3.5. Breakthrough curves modelling

For the fixed-bed adsorption process, the mathematical correlations of the breakthrough models depend largely on the external

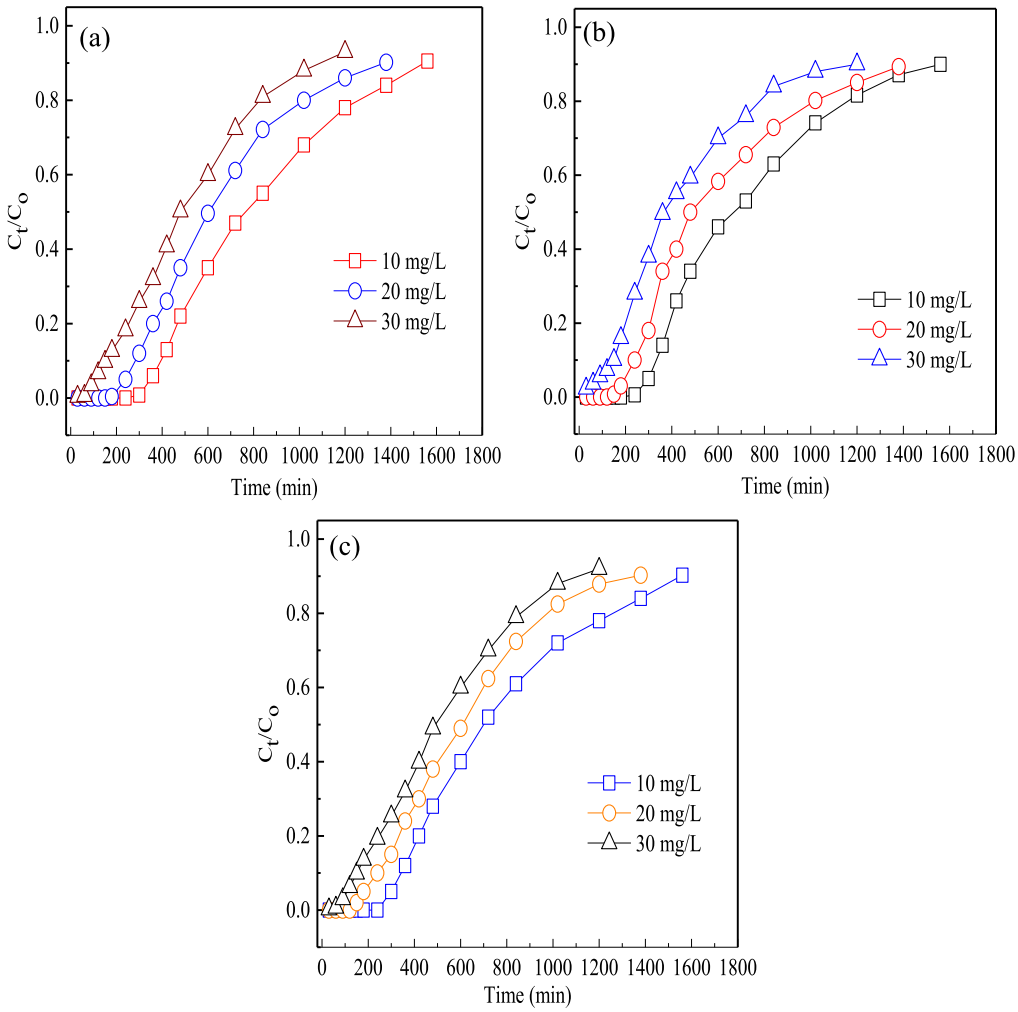

Fig. 7. The effect of inlet concentration on the breakthrough curve for the removal of (a) BOD; (b) COD and (c) TOC from the textile effluent at pH = 6.5 and temperature = 25 °C.

mass transfer, intraparticle diffusion and axial dispersion [77]. Fundamentally, breakthrough models predict the fixed-bed column behaviour and enhance the determination of the parameters required for successful design. Also, the evaluated parameters from the breakthrough models are vital for industrial-scale applications [56]. For this purpose, several mathematical models such as Thomas, Adams-Bohart and Yoon-Nelson have been established to analyze and describe the behaviour of the breakthrough curve utilizing the column set up at the laboratory scale. Specifically, the breakthrough curves for the fixed-bed adsorption performance of BOD, COD and TOC removal by MAGZA composite were fitted at various experimental data shown in Fig. 8(a–i) for the Thomas model and Fig. 9(a–i) for the Adams-Bohart and Yoon-Nelson models, respectively. In addition, the different parameters for each of the models were estimated and presented in Table 4. In all, the mathematical model's validity was evaluated using the correlation coefficient (R^2) and the Chi-square (X^2) statistical tool represented in Eqs. (8) and (9) [85].

$$R^2 = \frac{\sum (q_{mean} - q_{cal})^2}{\sum (q_{cal} - q_{mean})^2 + \sum (q_{cal} - q_{exp})^2} \tag{10}$$

$$\chi^2 = \sum \frac{(q_{exp} - q_{cal})^2}{q_{cal}} \tag{11}$$

3.5.1. Thomas model

Thomas model is ranked as the most widely used kinetic model for the efficiency of column operations predictions. Thomas model assumes that the rate driving force shows correspondence to the Langmuir adsorption isotherm of adsorption-desorption and the reversible second-order kinetics without axial dispersion [77]. Thomas model applies mostly to the performance evaluation of

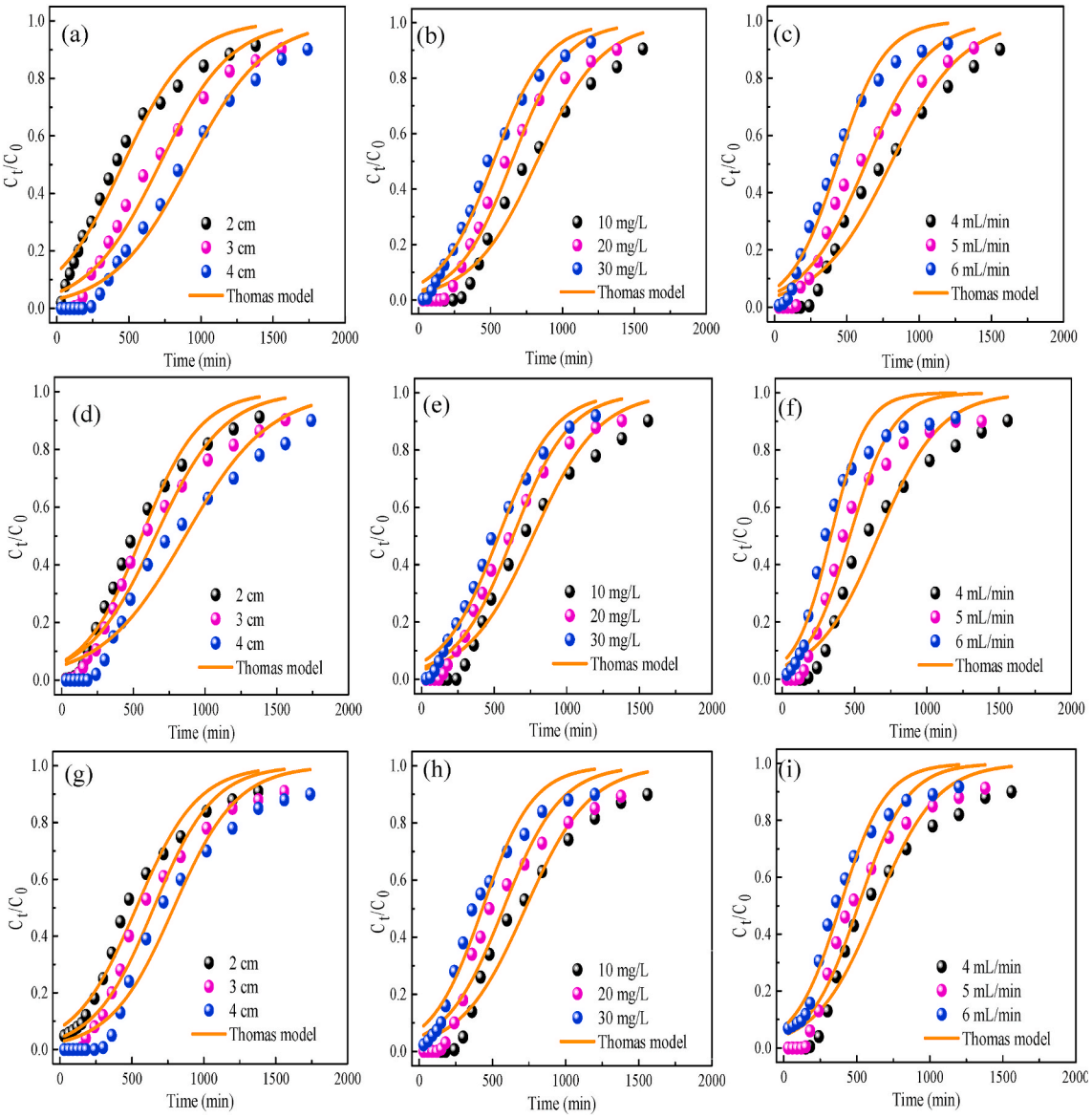

Fig. 8. The experimental and modeling curve of Thomas model for MAGZA composite removal of BOD at (a) bed height, (b) inlet concentration and (c) flow rate; COD removal at (d) bed height, (e) inlet concentration and (f) flow rate and TOC removal at (g) bed height, (h) inlet concentration and (i) flow rate.

continuous flow arrangement to predict the relationship between effluent concentration (C_t) and time (t) and is suitable for the adsorption process where negligible resistance exists between the internal and external diffusion [56]. The mathematical relationship for the Thomas model is given in Eq. (10) [3,81].

$$\ln\left(\frac{C_o}{C_t}-1\right)=\frac{K_{Th}q_0m}{Q}-K_{Th}C_0t \tag{12}$$

where C_0 (mg/L) and C_t (mg/L) refer to the inlet and effluent amounts (concentrations) of metal ions. Equally, k_{Th} (mL/(min.mg)) refers to the Thomas kinetic model constant, while q_0 (mg/g) is the adsorbed amount of BOD, COD and TOC at equilibrium conditions. Other parameters such as Q (mL/min) indicate the flow rate, while m (g) reveals the quantity of MAGZA composite in the column.

The breakthrough modelling curves of the experimental data fitted with the Thomas model at different flow rates, bed height and inlet adsorbate concentration were analyzed to determine the rate constant (k_{TH}) and the column adsorption capacity (q_o) as shown in Fig. 8(a–i). It is evident that the Thomas model suitably fitted the adsorption of BOD, COD and TOC by MAGZA composite in the fixed-bed column, indicating the non-limiting step of the internal and external diffusion [81]. Consequently, a lower adsorbate flow rate, higher bed height and lower adsorbate inlet concentration can effectively improve the removal capacity of BOD, COD and TOC by the

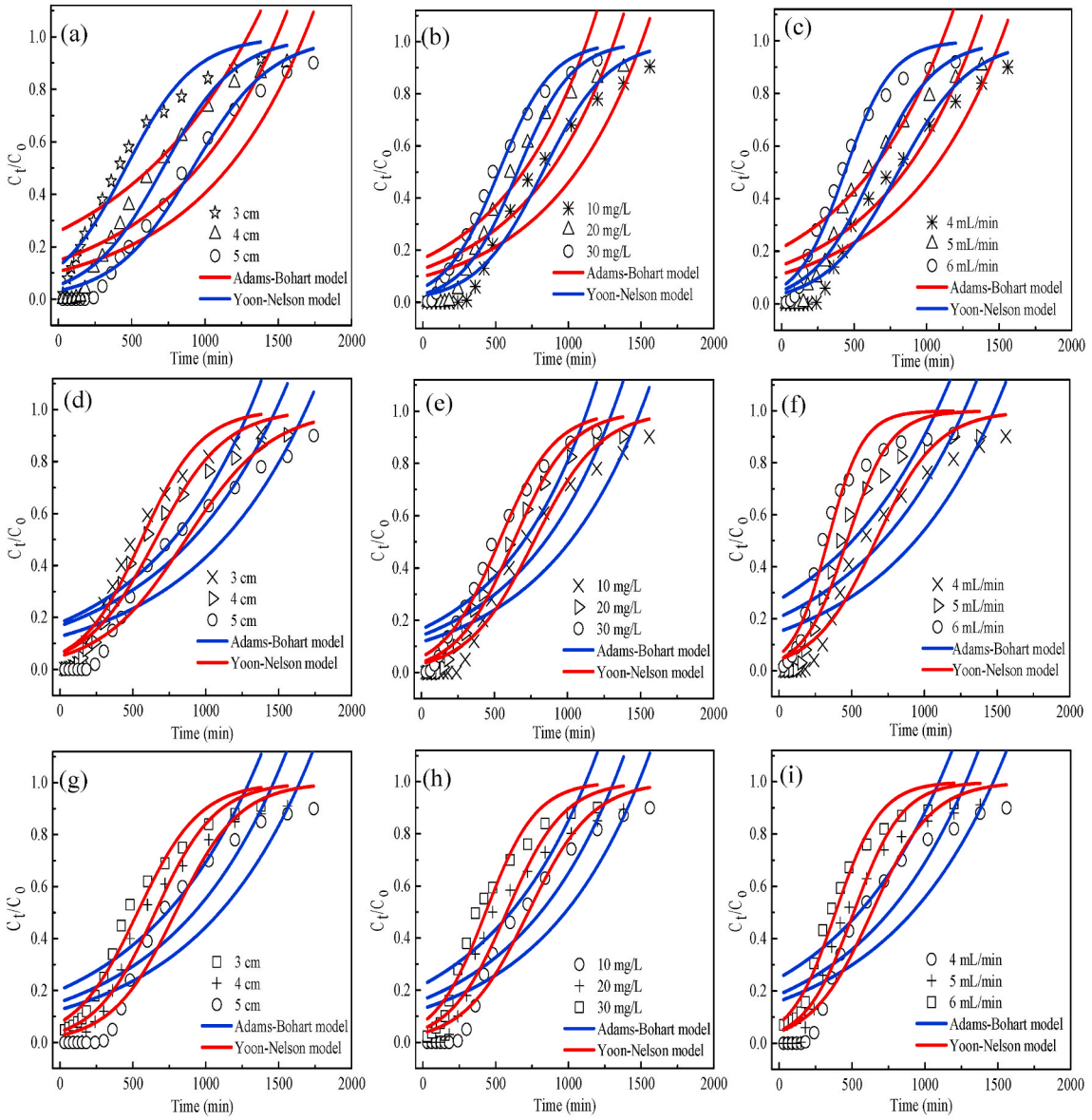

Fig. 9. The experimental and modeling curve of Adams-Bohart and Yoon-Nelson model for MAGZA composite removal of BOD at (a) bed height, (b) inlet concentration and (c) flow rate; removal of COD at (d) bed height, (e) inlet concentration and (f) flow rate and removal of TOC at (g) bed height, (h) inlet concentration and (i) flow rate.

MAGZA composite in the dynamic column. Notably, the parameters associated with the Thomas model, correlation coefficient (R^2) and Chi-square (X^2) were evaluated and presented in Table 4. Particularly in the BOD, COD and TOC adsorption, with an increase in the flow rate from 4 to 6 mL/min, the value of k_{TH} increased while the value of q_o significantly decreased which may be ascribed to the presence of the fixed amount of active sites and lack of sufficient contact time between the adsorbate and the adsorbent [86,87]. Moreover, increasing the bed height from 3 to 5 cm decreased and increased the values of k_{TH} and q_o respectively. The increase of the k_{TH} may be attributed to the increase in the driving force of mass concentration with increasing bed height, while the decrease in the q_o may be due to an increase in the flow resistance that results in a decline in the effect of mass transfer [56]. On the other hand, the values of k_{TH} decreased significantly as the adsorbate inlet concentration increased from 10 to 30 mg/L, while the values of q_o increased for all the adsorbates. Overall, the observed increment in the q_o may be linked to the existence of a concentration gradient that acts as the driving force for improved adsorption [80]. In addition, the values of R^2 and X^2 in Table 4 revealed close conformity of the Thomas model to the experimental data compared to the Adams-Bohart model.

3.5.2. Adams-Bohart model

Adams-Bohart model relates to the initial conditions of the breakthrough curve for the adsorption wastewater. The key assumption

Table 4
Determined parameters from Thomas, Adams-Bohart and Yoon-Nelson models for the adsorption of BOD, COD and TOC by MAGZA composite.

Adsorbate	Q (mL.min^{-1})	H (cm)	C_o (mg.L^{-1})	Thomas				Adams-Bohart				Yoon-Nelson			
				k_{TH}	q_o	R^2	X^2	K_{AB}	N_o	R^2	X^2	K_{YN}	τ	R^2	X^2
BOD	4	3	10	0.00425	194.89	0.958	0.0038	0.00145	1352	0.757	0.0220	0.00322	458.48	0.958	0.0038
	4	4	10	0.00402	286.61	0.965	0.0038	0.00139	1913	0.804	0.0215	0.00306	712.32	0.965	0.0038
	4	5	10	0.00372	364.50	0.980	0.0021	0.00134	2246	0.848	0.0169	0.00260	915.34	0.980	0.0021
	4	5	20	0.00540	281.82	0.971	0.0034	0.00156	2055	0.786	0.0251	0.00530	649.24	0.971	0.0034
	4	5	30	0.00530	344.19	0.982	0.0019	0.00158	1786	0.805	0.0211	0.00540	521.73	0.982	0.0019
	5	5	10	0.00468	294.84	0.958	0.0046	0.00140	1924	0.788	0.0234	0.00468	630.56	0.958	0.0046
	6	5	10	0.00616	268.12	0.969	0.0035	0.00146	1546	0.730	0.0309	0.00616	434.96	0.969	0.0035
COD	4	3	10	0.00488	272.55	0.960	0.0044	0.00132	1718	0.763	0.0264	0.00488	558.80	0.960	0.0044
	4	4	10	0.00420	275.42	0.959	0.0046	0.00127	1786	0.775	0.0249	0.00420	655.58	0.959	0.0046
	4	5	10	0.00440	338.32	0.949	0.0055	0.00122	2063	0.811	0.0203	0.00340	862.42	0.949	0.0055
	4	5	20	0.00521	276.82	0.976	0.0027	0.00150	1958	0.792	0.0240	0.00509	630.34	0.976	0.0027
	4	5	30	0.00509	320.57	0.979	0.0021	0.00159	1798	0.809	0.0199	0.00521	531.15	0.979	0.0021
	5	5	10	0.00671	313.77	0.953	0.0062	0.00125	1584	0.676	0.0427	0.00671	467.78	0.953	0.0062
	6	5	10	0.00824	276.74	0.950	0.0061	0.00129	1296	0.621	0.0463	0.00824	335.88	0.950	0.0061
TOC	4	3	10	0.00470	249.31	0.968	0.0033	0.00133	1596	0.769	0.0240	0.00470	530.81	0.968	0.0033
	4	4	10	0.00481	313.94	0.963	0.0046	0.00127	1860	0.762	0.0294	0.00481	652.32	0.963	0.0046
	4	5	10	0.00454	359.44	0.961	0.0051	0.00126	2071	0.773	0.0296	0.00454	791.25	0.961	0.0051
	4	5	20	0.00576	248.97	0.937	0.0074	0.00135	1811	0.734	0.0310	0.00510	575.58	0.937	0.0074
	4	5	30	0.00510	293.72	0.953	0.0050	0.00138	1510	0.721	0.0299	0.00576	431.93	0.953	0.0050
	5	5	10	0.00598	305.67	0.951	0.0063	0.00126	1681	0.707	0.0373	0.00598	511.12	0.951	0.0063
	6	5	10	0.00648	250.82	0.966	0.0037	0.00131	1387	0.699	0.0331	0.00648	386.76	0.966	0.0037

of the model is the non-instantaneous nature of the adsorption reaction, in which the adsorption rate shows proportionality to the residual adsorbent capacity and the gaseous concentration of the adsorbate [60]. The mathematical definition of the Adams-Bohart model is presented in Eq. (11) [56,88].

$$\ln\left(\frac{C_t}{C_o}\right) = K_{AB}C_0 t - \left(\frac{K_{AB}N_0 H}{u}\right) \tag{13}$$

in which K_{AB} (mL/min mg) and N_0 (mg/L) are kinetic rates constant of the Adams-Bohart model and the concentration at saturation. The parameters, H (cm) and u (cm/min) show the height of the fixed-bed depth occupied with MAGZA composite and inlet gas linear velocity, respectively.

Further analysis of the breakthrough modelling curves was conducted by fitting the experimental data to the Adams-Bohart model at the various flow rate, bed height and inlet concentrations as demonstrated in Fig. 9(a–i) representing the experimental and predicted breakthrough curves. Importantly, the Adams-Bohart kinetic constant (k_{AB}) and the saturation concentration (N_0) are obtainable in the range of $0.1 < (C_t/C_o) < 0.9$. The calculated values of Adams-Bohart parameters (k_{AB} and N_0), along with the statistical parameters (R^2 and X^2) of the breakthrough curves modelling analysis are presented in Table 4. Following the model parameters shown in Table 4, the values of k_{AB} for the BOD, COD and TOC adsorption by the MAGZA composite were observed to increase significantly with an increase in the adsorbate flow rate and the inlet concentration. Similarly, an increase in the adsorbate flow rate and the inlet concentration significantly decreased the values of N_0 for the adsorption of BOD, COD and TOC, respectively and may be attributed to quicker bed saturation due to higher pollutant loading from the flow rate increment [32,80]. However, the values of k_{AB} decreased with the increasing bed height, while the values of N_0 noticeably increased with the increase in the bed depth due to the large availability of active sites for the BOD, COD and TOC adsorption [81,82]. For the statistical evaluation, the high values obtained for the R^2 and X^2 indicated the non-suitability of the Adams-Bohart model to predict the breakthrough curve.

3.5.3. Yoon-Nelson model

Yoon-Nelson model is regarded as a considerably simplified model for volatile/gaseous adsorbates removal onto adsorbents, thereby enabling breakthrough curve prediction. The model assumptions are based on the circumstance that the expected decline in the rate of the adsorption of each accounted molecule of adsorbate corresponds to an adsorbent breakthrough [89]. Yoon-Nelson model does not require inputs interrelated to the adsorbate characteristics, adsorbent type and adsorption bed physical properties, thereby making it as non-complicated as other models. The Yoon-Nelson model is expressed in Eq. (12) [77,90].

$$\ln\left(\frac{C_t}{C_o - C_t}\right) = k_{YN}t - \tau k_{YN} \tag{14}$$

in all, k_{YN} (1/min) and τ are the kinetic constants of the model and the time required to achieve a 50% breakthrough.

The analysis of the experimental and predicted breakthrough curves was performed by fitting the data obtained from the experiment to the Yoon-Nelson model at the different flow rates, bed depth and inlet concentration as shown in Fig. 9(a–i). The evaluation of Yoon-Nelson parameters (k_{YN} and τ) and the statistical parameters (R^2 and X^2) were carried out and presented in Table 4. The fitting parameters of the Yoon-Nelson model indicate that by increasing the adsorbate flow rate and the adsorbate inlet concentration, the

Table 5
Characterization of raw and treated textile wastewater compared with WHO and US EPA standards.

Parameters	Raw Value	Treated with MAGZA composite	Removal of Pollutants (%)	WHO/EPA Standard Limit
BOD (mg/L)	6287	2.4	99.96	-/5.0–7.0
COD (mg/L)	31044	36	99.88	-/40
TOC (mg/L)	2990	4	99.87	-/<6
TDS (mg/L)	36723	500	98.64	1000/-
pH	11.40	6.5	42.98	6.0–8.5/6.0–9.5
Conductivity (μS/cm)	54810	860	98.43	-/1000
Turbidity (NTU)	7638	75	99.02	5.0
Total alkalinity (mg/L)	16443	320	98.05	-/400
Nitrate (mg/L)	1804	20	98.89	50/50
Ammonia (mg/L)	276	3.5	98.73	1.3–3.5/0.2–4.0
Chloride (mg/L)	9711	31	99.68	250/250
Phosphate (mg/L)	113	0.5	99.56	-/0.5-0.7
Fluoride (mg/L)	226	1.48	99.35	1.5/1.7
Sulphate (mg/L)	7111	25	99.65	500/250
Iron (mg/L)	3.64	0.05	98.63	-/0.3
Chromium (mg/L)	2.12	0.03	98.58	0.05/0.05
Nickel (mg/L)	1.45	0.001	99.93	0.07/0.02
Zinc (mg/L)	1.14	0.007	99.39	-/3
Lead (mg/L)	3.75	0.005	99.87	0.01/0.01
Cadmium (mg/L)	2.54	0.003	99.88	0.003
Copper (mg/L)	2.13	0.002	99.91	2/1
Manganese (mg/L)	1.12	0.002	99.82	-/0.2

value of k_{YN} increased significantly, while the value of τ decreased for the adsorption of BOD, COD and TOC by MAGZA composite. This trend may be ascribed to the quick saturation of the adsorbent present in the column due to the increasing concentration gradient across the bed [82]. Then again, an increase in the bed depth resulted in a remarkable decline in the value of k_{YN} and an increase in the value of τ. The observed variations may be due to the increase in the number of adsorbents in the bed that provide abundant adsorption sites for the removal of BOD, COD and TOC [56]. Overall, the values obtained from the R^2 and X^2 reveal that both Thomas and Yoon-Nelson models can be utilized effectively for the prediction of the breakthrough curves of BOD, COD and TOC adsorption due to the high values of the R^2 close to unity and the low values of the X^2, compared to Adams-Bohart model. Remarkably, a good fitting of the experimental data to kinetic models reveals the characteristics of the column adsorption mechanism. In Table 4, the values of R^2 and X^2 were the same, indicating the prediction of similar breakthrough curves by both models in the adsorption process. The results of this study show correspondence with the previous result of other researchers [56,79,80,82].

3.6. Water quality parameters

Herein, the water quality parameters such as BOD, COD, TOC, TDS, pH, conductivity, turbidity, total alkalinity, nitrate, ammonia, chloride, phosphate, fluoride, sulphate, iron, chromium, nickel, zinc, lead, cadmium, copper and manganese concentrations were evaluated before and after treatment with MAGZA composite and compared with WHO and EPA standards as shown in Table 5. After the treatment of wastewater using MAGZA composite, the values of the BOD, COD, TOC, TDS, conductivity and turbidity reduced to fall within the permissible concentrations recommended by WHO and EPA.

In addition, a decline in the concentrations of phosphate (0.5 mg/L), fluoride (1.48 mg/L), sulphate (25 mg/L), iron (0.05 mg/L), chromium (0.03 mg/L), nickel (0.001 mg/L), zinc (0.07 mg/L), lead (0.005 mg/L), cadmium (0.003 mg/L), copper (0.002 mg/L) and

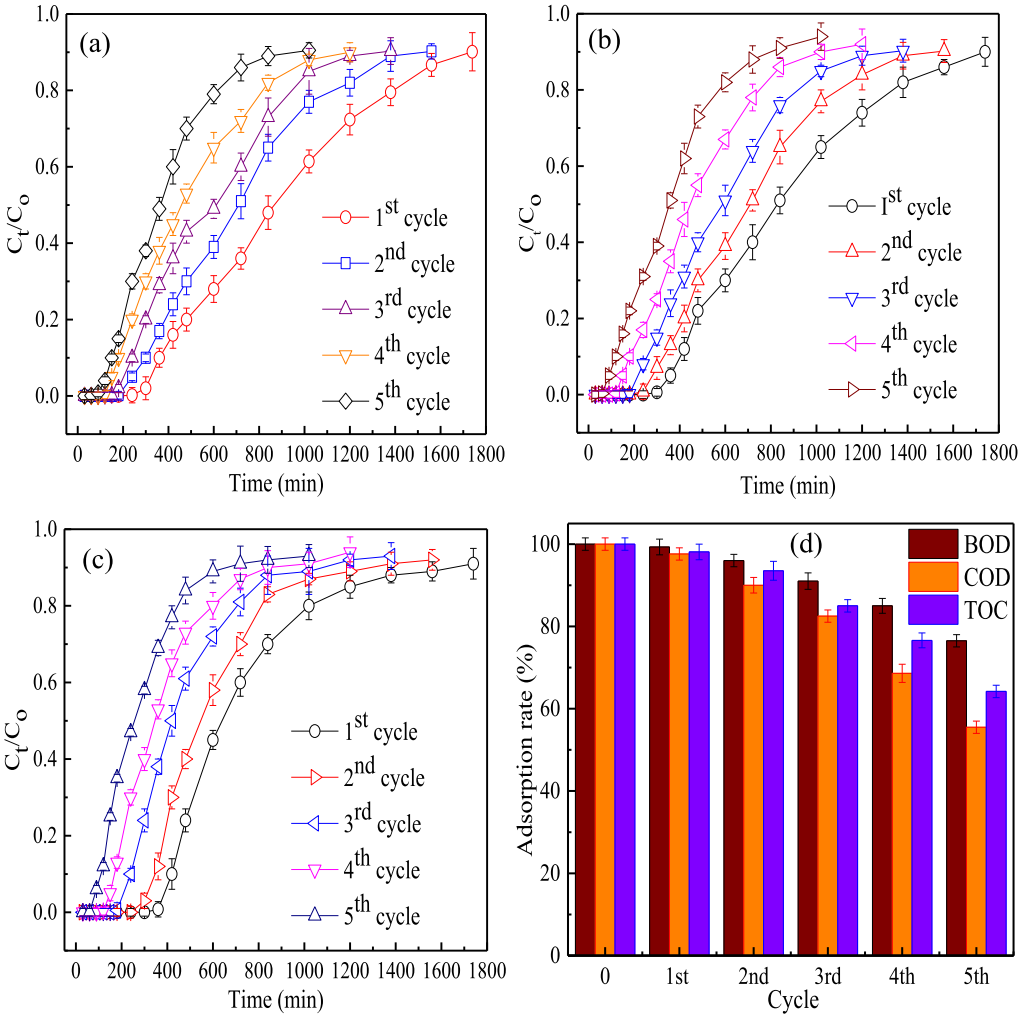

Fig. 10. Reusability investigation of MAGZA composite for the adsorption of (a) BOD; (b) COD; (c) TOC in a fixed-bed column and (d) the percentage adsorption rate at each cycle.

manganese (0.002 mg/L) was observed after treatment using MAGZA composite. Overall, the concentrations obtained for the water parameters fall within the permissible concentration limit recommended by US EPA and WHO [54,55]. In all, all the water parameters presented in Table 5 recorded over 98% removal capacity, except pH which indicated 42.98% removal capacity. More so, the MAGZA composite adsorbent has octahedral sites at the surface of the crystal structure that made binding easier [45]. In the end, the treated water showed suitability for drinking and other domestic applications.

3.7. Regeneration and reusability

The regeneration attributes of adsorbents determine greatly the cost efficiency of adsorption operation and reuse to minimize the output of solid wastes [38]. Hence, the regeneration and reusability capacity of MAGZA composite in a fixed-bed adsorption column was examined and the results are illustrated in Fig. 10(a,b,c). In all, the reuse study of the adsorbent was conducted in five cycles for the removal of BOD, COD and TOC in a fixed-bed column. As evident from Fig. 10(a,b,c), successive increases in the reusability cycle revealed a decline in the breakthrough time (t_b) and exhaustion time (t_e) which shifts the breakthrough curves towards the left. Particularly after the 1st, 2nd, 3rd, 4th and 5th cycle operation, the obtained t_b are 360, 300, 240, 180 and 150 min for BOD adsorption, 420, 360, 300, 240 and 180 min for COD adsorption and 420, 360, 240, 180 and 150 min for TOC adsorption, respectively as shown in Fig. 10(a,b,c). Similarly, the t_e noticeably reduced for BOD (1740, 1560, 1380, 1200 and 1020 min), COD (1740, 1560, 1380, 1020 and 840 min) and TOC (1560, 1380, 1020, 840 and 720 min) after the 1st, 2nd, 3rd, 4th and 5th adsorption cycle, respectively. The observed reduction may be ascribed to the gradual blockage of the active sites of the MAGZA composite with an increasing reusability cycle [56]. In the end, the adsorption of BOD, COD and TOC reduced to 77, 56 and 64% after the 5th adsorption cycle as shown in Fig. 10(d). Overall, the relatively high effectiveness of the composite after the 5th cycle reveals its potential feasibility and stability for industrial applicability.

3.8. Comparative study

Generally, it is challenging to obtain an effective, simple and economical separation process that can remove different organic pollutants, inorganic pollutants and heavy metals from industrial wastewater. The continuous adsorption system explored in this study enhanced the contact of the low quantity of the prepared MAGZA adsorbent and the contaminated textile wastewater to achieve efficient removal of the pollutants. As such, there will be cost minimization and conservation of space to handle large amounts of effluents that do not involve the consumption of energy and monitoring. Compared with the various adsorbents used previously over the literation as shown in Table 6, the MAGZA composites fixed-bed adsorption column showed remarkable effectiveness, cost-efficient, ease of operation, recyclable and scalable to industrial application in the removal of real industrial wastewater. Overall, the removal efficiency of the pollutants was effective and relatively over 98% (except pH of 42.98%) compared to the previously used adsorbents and presents considerable effectiveness in the treatment of industrial wastewater.

4. Conclusions

In this study, the magnetite/zeolite A (MAGZA) composite was effectively fabricated by the decoration of the magnetite NPs onto the surface matrix of zeolite A. The results from the characterization techniques indicated the presence of surface functional groups, crystallinity, microstructural morphology and surface properties characteristic of magnetite NPs, zeolite A and MAGZA composite. The surface area of 95.26 ± 2, 119.98 ± 3 and 110.50 ± 6 m^2/g were recorded for the magnetite NPs, zeolite A and MAGZA composite, respectively. The comparative investigation of adsorbents selectivity towards BOD, COD and TOC demonstrated a maximum adsorption capacity of 255.98, 241.94 and 243.36 mg/g using magnetite NPs; 323.66, 295.79 and 302.92 mg/g using zeolite A and 385.86, 330.10 and 374.01 mg/g using MAGZA composite. MAGZA composite with higher adsorption capacity was further used for experimental investigation of BOD, COD and TOC removal from textile wastewater in a fixed-bed adsorption method considering the influence of parameters such as flow rate, adsorbent bed height and adsorbate inlet concentration. Overall, the adsorption results indicate that the breakthrough time, exhaustion time and adsorbate percentage removal increased considerably with an increase in the adsorbent bed height within the column. However, the increase in flow rate and adsorbate inlet concentration considerably declined the breakthrough time, exhaustion time and adsorbate percentage removal. Notably, maximum performance of the fixed bed column using MAGZA was obtained for BOD (t_b = 360 min, t_e = 1740 min and %R = 99.96%), COD (t_b = 300 min, t_e = 1700 min and %R = 99.88%) and TOC (t_b = 420 min, t_e = 1680 min and %R = 99.87%) at the bed height of 5 cm, flow rate of 4 mL/min and adsorbate inlet concentration of 10 mg/L. Thomas and Yoon-Nelson models exhibited better fitting to the breakthrough curves of the MAGZA composite bed column compared to the Adams-Bohart model. The MAGZA composite showed the capacity to be reused five times in a fixed-bed column. Therefore, the MAGZA composite can be a promising and cost-efficient alternative adsorbent for the removal of organic and inorganic contaminants from textile wastewater in a highly scalable industrial fixed-bed adsorption method.

Author contribution statement

Abdulsalami Sanni Kovo, Sherifat Alaya-Ibrahim: Conceived and designed the experiments; Performed the experiments; Contributed reagents, materials, analysis tools or data; Wrote the paper.

Ambali Saka Abdulkareem: Conceived and designed the experiments; Performed the experiments; Analyzed and interpreted the data; Contributed reagents, materials, analysis tools or data; Wrote the paper.

Table 6
Comparison of various adsorbents removal efficiency towards various pollutants.

Adsorbents	Pollutants	Study type	Treated water	Removal Efficiency (%)	Reference
CuO@activated carbon (AC) composite	BOD, COD and TOC	Advanced oxidation process	Textile wastewater	BOD (70%), COD (72%) and TOC (61%)	[8]
Vetiveria zizanioides	BOD, COD and TDS	Floating phyto-bed reactor	Textile wastewater	BOD (81%), COD (74%) and TDS (66%)	[91]
Nano Zero-Valent Iron	COD and Turbidity	Batch adsorption	Textile wastewater	BOD (97.3%) and Turbidity (85.7 NTU)	[30]
SBA-15/GO	Turbidity, TOC, colour, TSS, COD, BOD, NO_3^{2-}, TP, Ni, Fe, Pb, Cu, Cr, and Cd	Continuous adsorption	Industrial wastewater	Turbidity(99.24%), TOC(97.02%), color(94.80%), TSS(94.36%), COD (98.66%), BOD(98.46), NO_3^{2-} (98.35%), TP(96.43%), Ni(100), Fe (99.73%), Pb (90.85%), Cu(81.73%), Cr(63.68%) and Cd(66.67%)	[77]
Bagasse based fly ash	COD TOC	Electrochemical + continuous adsorption	Sugar industry wastewater	COD (91.93%)	[51]
$Fe^{2+}/Fe^{3+}/Co^{2+}$ cocatalysts	COD and TOC	Electo-fenton process	Pharmaceutical wastewater	COD (93%) and TOC (92%).	[92]
Tea waste biochar	COD	Batch adsorption	Produced water	COD (95.5%)	[7]
Sand, SAC	BOD, COD and TDS	Continuous adsorption	Greywater	BOD (93.4%), COD (82.7%) and TDS (96.5%)	[3]
$Al_2(SO_4)_3$	COD and TOC	Chemical Coagulation-Electro-Oxidation	Textile wastewater	COD (93.5%) and TOC (75%)	[93]
Nano-calcite ($CaCO_3$)	COD, BOD and TOC	Photocatalytic degradation	Industrial effluents	COD (78.5%), BOD (77.6%) and TOC (64.5%)	[50]
Graphene oxide	Turbidity and COD	Continuous adsorption	Textile wastewater	Turbidity (90%) and COD (60.9%)	[94]
Single-Walled and multi-walled CNTs	COD, TOC and TDS	Continuous adsorption	Effluent treatment plant	COD (39.58%), TDS (66.86%), and TOC (85.88%)	[95]
Granular Al–Mn binary oxide-zeolite composite	Ammonia and Phosphate	Continuous adsorption	Simulated wastewater	Ammonia (56.14%) and phosphate (76.41%)	[96]
MAGZA composite	BOD, COD, TOC, TDS, pH, conductivity, turbidity, total alkalinity, nitrate, ammonia, chloride, phosphate and fluoride, sulphate.	Continuous adsorption	Textile wastewater	BOD (99.96%), COD (99.88%), TOC (99.87%), TDS (98.64%), pH (42.98%), conductivity (98.43%), turbidity (99.02%), nitrate (98.89%), ammonia (98.73%), chloride (99.68%), phosphate (99.56%), fluoride (99.35%) and sulphate (99.65%)	This study

Olalekan David Adeniyi: Conceived and designed the experiments; Performed the experiments; Analyzed and interpreted the data; Contributed reagents, materials, analysis tools or data.

Titus Chinedu Egbosiuba: Conceived and designed the experiments; Analyzed and interpreted the data; Wrote the paper.

Jimoh Oladejo Tijani, Blessing Onyinye Okafor, Yusuff Sikiru Adeyinka: Performed the experiments; Analyzed and interpreted the data; Contributed reagents, materials, analysis tools or data.

Saheed Mustapha: Performed the experiments; Analyzed and interpreted the data; Contributed reagents, materials, analysis tools or data; Wrote the paper.

Funding statement

This research did not receive any specific grant from funding agencies in the public, commercial, or not-for-profit sectors.

Data availability statement

Data will be made available on request.

Declaration of interest's statement

The authors declare no competing interests.

Appendix A. Supplementary data

Supplementary data related to this article can be found at https://doi.org/10.1016/j.heliyon.2023.e13095.

References

[1] M.S.B. Khalith, R. Rishabb Anirud, R. Ramalingam, S.K. Karuppannan, M.J.H. Dowlath, K. Pandion, B. Ravindran, S. WoongChang, D. Ovi, M.V. Arasu, S. Ignacimuthu, N.A. Al-Dhabi, M. Chandrasekaran, K.D. Arunachalam, Synthesis and characterization of magnetite carbon nanocomposite from agro waste as chromium adsorbent for effluent treatment, Environ. Res. 202 (2021), 111669, https://doi.org/10.1016/j.envres.2021.111669.

[2] M.W. Letshwenyo, T.V. Sima, Phosphorus removal from secondary wastewater effluent using copper smelter slag, Heliyon 6 (2020), e04134, https://doi.org/10.1016/j.heliyon.2020.e04134.

[3] P. Patel, S. Gupta, P. Mondal, Modeling of continuous adsorption of greywater pollutants onto sawdust activated carbon bed integrated with sand column, J. Environ. Chem. Eng. 10 (2022), 107155, https://doi.org/10.1016/j.jece.2022.107155.

[4] UN, UN-Water, Summary Progress Update 2021: SDG 6 — water and sanitation for all, UN-Water, 1–58, https://www.unwater.org/new-data-on-global-progresstowards-%0Aensuring-water-and-sanitation-for-all-by-2030/, 2021.

[5] T. Chinedu Egbosiuba, Application of Agricultural Waste in Anionic Dyes Removal from Wastewater, Springer, Singapore, 2022, https://doi.org/10.1007/978-981-19-2852-9_7.

[6] S. Sagadevan, I. Fatimah, T.C. Egbosiuba, S.F. Alshahateet, J.A. Lett, G.K. Weldegebrieal, M.V. Le, M.R. Johan, Photocatalytic efficiency of titanium dioxide for dyes and heavy metals removal from wastewater, Bull. Chem. React. Eng. Catal. 17 (2022) 430–450, https://doi.org/10.9767/BCREC.17.2.13948.430-450.

[7] H. Khurshid, M.R.U. Mustafa, U. Rashid, M.H. Isa, Y.C. Ho, M.M. Shah, Adsorptive removal of COD from produced water using tea waste biochar, Environ. Technol. Innovat. 23 (2021), 101563, https://doi.org/10.1016/j.eti.2021.101563.

[8] R. Kiani, F. Mirzaei, F. Ghanbari, R. Feizi, F. Mehdipour, Real textile wastewater treatment by a sulfate radicals-Advanced Oxidation Process: peroxydisulfate decomposition using copper oxide (CuO) supported onto activated carbon, J. Water Proc. Eng. 38 (2020), 101623, https://doi.org/10.1016/j.jwpe.2020.101623.

[9] S. De Gisi, M. Notarnicola, Industrial Wastewater Treatment, 2017, https://doi.org/10.1016/B978-0-12-409548-9.10167-8.

[10] Y. Ibrahim, V. Naddeo, F. Banat, S.W. Hasan, Preparation of novel polyvinylidene fluoride (PVDF)-Tin(IV) oxide (SnO2) ion exchange mixed matrix membranes for the removal of heavy metals from aqueous solutions, Separ. Purif. Technol. 250 (2020), 117250, https://doi.org/10.1016/j.seppur.2020.117250.

[11] C. Vaneeckhaute, O. Darveau, E. Meers, Fate of micronutrients and heavy metals in digestate processing using vibrating reversed osmosis as resource recovery technology, Separ. Purif. Technol. 223 (2019) 81–87, https://doi.org/10.1016/j.seppur.2019.04.055.

[12] D.Q. Cao, X. Wang, Q.H. Wang, X.M. Fang, J.Y. Jin, X. Di Hao, E. Iritani, N. Katagiri, Removal of heavy metal ions by ultrafiltration with recovery of extracellular polymer substances from excess sludge, J. Membr. Sci. 606 (2020), 118103, https://doi.org/10.1016/j.memsci.2020.118103.

[13] C.A. Igwegbe, S.N. Oba, C.O. Aniagor, A.G. Adeniyi, J.O. Ighalo, Adsorption of ciprofloxacin from water: a comprehensive review, J. Ind. Eng. Chem. 93 (2021) 57–77, https://doi.org/10.1016/j.jiec.2020.09.023.

[14] E. Sodaitienė, A. Gefenienė, D. Kaušpėdienė, R. Ragauskas, J. Vaičiūnienė, A. Selskienė, V. Jasulaitienė, R. Ramanauskas, Sustainable removal of anodized aluminum dye by groundwater treatment waste: experimental and modeling, Heliyon 7 (2021), https://doi.org/10.1016/j.heliyon.2021.e05993.

[15] P.L. Homagai, R. Poudel, S. Poudel, A. Bhattarai, Adsorption and removal of crystal violet dye from aqueous solution by modified rice husk, Heliyon 8 (2022), e09261, https://doi.org/10.1016/j.heliyon.2022.e09261.

[16] M. Fathy, M.A. Zayed, Y.M. Moustafa, Synthesis and applications of CaCO3/HPC core–shell composite subject to heavy metals adsorption processes, Heliyon 5 (2019), e02215, https://doi.org/10.1016/j.heliyon.2019.e02215.

[17] J.O. Tijani, M.N. Abdullahi, M.T. Bankole, S. Mustapha, T.C. Egbosiuba, M.M. Ndamitso, A.S. Abdulkareem, E. Muzenda, Photocatalytic and toxicity evaluation of local dyeing wastewater by aluminium/boron doped WO3 nanoparticles, J. Water Proc. Eng. 44 (2021), 102376, https://doi.org/10.1016/j.jwpe.2021.102376.

[18] J.O. Tijani, E.I. Odeh, S. Mustapha, T.C. Egbosiuba, A.I. Daniel, A.S. Abdulkareem, F.N. Muya, Photocatalytic, electrochemical, antibacterial and antioxidant behaviour of carbon-sulphur Co-doped zirconium (IV) oxide nanocomposite, Clean. Chem. Eng. 3 (2022), 100034, https://doi.org/10.1016/j.clce.2022.100034.

[19] L. Li, J. Zhang, Y. Li, C. Yang, Removal of Cr (VI) with a spiral wound chitosan nanofiber membrane module via dead-end filtration, J. Membr. Sci. 544 (2017) 333–341, https://doi.org/10.1016/j.memsci.2017.09.045.

[20] T.C. Egbosiuba, Incorporation of zero-valent silver and polyvinyl acetate on the surface matrix of carbon nanotubes for the adsorption of mercury and chromium from industrial wastewater, Niger, J. Technol. 41 (2022) 158–168, https://doi.org/10.4314/njt.v41i1.20.

[21] T.C. Egbosiuba, A.S. Abdulkareem, A.S. Kovo, E.A. Afolabi, J.O. Tijani, W.D. Roos, Enhanced adsorption of As(V) and Mn(VII) from industrial wastewater using multi-walled carbon nanotubes and carboxylated multi-walled carbon nanotubes, Chemosphere 254 (2020), 126780, https://doi.org/10.1016/j.chemosphere.2020.126780.

[22] T.C. Egbosiuba, A.S. Abdulkareem, A.S. Kovo, E.A. Afolabi, J.O. Tijani, M.T. Bankole, S. Bo, W.D. Roos, Adsorption of Cr(VI), Ni(II), Fe(II) and Cd(II) ions by KIAgNPs decorated MWCNTs in a batch and fixed bed process, Sci. Rep. 11 (2021) 1–20, https://doi.org/10.1038/s41598-020-79857-z.

[23] T.C. Egbosiuba, A.S. Abdulkareem, J.O. Tijani, J.I. Ani, V. Krikstolaityte, M. Srinivasan, A. Veksha, G. Lisak, Taguchi optimization design of diameter-controlled synthesis of multi walled carbon nanotubes for the adsorption of Pb(II) and Ni(II) from chemical industry wastewater, Chemosphere 266 (2021), https://doi.org/10.1016/j.chemosphere.2020.128937.

[24] C.A. Uko, J.O. Tijani, S.A. Abdulkareem, S. Mustapha, T.C. Egbosiuba, E. Muzenda, Adsorptive properties of MgO/WO3 nanoadsorbent for selected heavy metals removal from indigenous dyeing wastewater, Process Saf. Environ. Protect. 162 (2022) 775–794, https://doi.org/10.1016/j.psep.2022.04.057.

[25] S.M. Al-Jubouri, H.A. Al-Jendeel, S.A. Rashid, S. Al-Batty, Antibiotics adsorption from contaminated water by composites of ZSM-5 zeolite nanocrystals coated carbon, J. Water Proc. Eng. 47 (2022), 102745, https://doi.org/10.1016/j.jwpe.2022.102745.

[26] Z. Mo, D. Tai, H. Zhang, A. Shahab, A comprehensive review on the adsorption of heavy metals by zeolite imidazole framework (ZIF-8) based nanocomposite in water, Chem. Eng. J. (2022), 136320, https://doi.org/10.1016/j.cej.2022.136320.

[27] A.G. Adeniyi, J.O. Ighalo, Biosorption of pollutants by plant leaves: an empirical review, J. Environ. Chem. Eng. 7 (2019), 103100, https://doi.org/10.1016/j.jece.2019.103100.

[28] T.C. Egbosiuba, Biochar and bio-oil fuel properties from nickel nanoparticles assisted pyrolysis of cassava peel, Heliyon 8 (2022), e10114, https://doi.org/10.1016/j.heliyon.2022.e10114.

[29] S. Mahajan, V. Srivastava, M. Sillanpää, Novel poly-D-galacturonic acid methyl ester grafted vinyl monomer polymer super green adsorbent via C-O strategic protrusion of methyl methacrylate (MMA) for removal of Sm (III) and Nd (III), Separ. Purif. Technol. 258 (2021), 117474, https://doi.org/10.1016/j.seppur.2020.117474.

[30] A.K. Badawi, K. Zaher, Engineering Hybrid treatment system for real textile wastewater remediation based on coagulation/flocculation , adsorption and filtration processes : performance and economic evaluation, J. Water Proc. Eng. 40 (2021), 101963, https://doi.org/10.1016/j.jwpe.2021.101963.

[31] A.M. Álvarez, D.B. Guerrón, C. Montero Calderón, Natural zeolite as a chromium VI removal agent in tannery effluents, Heliyon 7 (2021), https://doi.org/10.1016/j.heliyon.2021.e07974.

[32] T.C. Egbosiuba, M.C. Egwunyenga, J.O. Tijani, S. Mustapha, A.S. Abdulkareem, A.S. Kovo, V. Krikstolaityte, A. Veksha, M. Wagner, G. Lisak, Activated multi-walled carbon nanotubes decorated with zero valent nickel nanoparticles for arsenic, cadmium and lead adsorption from wastewater in a batch and continuous flow modes, J. Hazard Mater. 423 (2022), 126993, https://doi.org/10.1016/j.jhazmat.2021.126993.

[33] C.H. Pérez-Beltrán, J.J. García-Guzmán, B. Ferreira, O. Estévez-Hernández, D. López-Iglesias, L. Cubillana-Aguilera, W. Link, N. Stănică, A.M. Rosa da Costa, J. M. Palacios-Santander, One-minute and green synthesis of magnetic iron oxide nanoparticles assisted by design of experiments and high energy ultrasound: application to biosensing and immunoprecipitation, Mater. Sci. Eng. C 123 (2021), https://doi.org/10.1016/j.msec.2021.112023.

[34] P. Karpagavinayagam, A. Emi Princess Prasanna, C. Vedhi, Eco-friendly synthesis of nickel oxide nanoparticles using Avicennia Marina leaf extract: morphological characterization and electrochemical application, Mater. Today Proc. (2020), https://doi.org/10.1016/j.matpr.2020.04.183.

[35] H. Ghorbani, M. Eshraghi, A.A. Sabouri Dodaran, Structural and magnetic properties of cobalt ferrite nanoparticles doped with cadmium, Phys. B Condens. Matter 634 (2022), 413816, https://doi.org/10.1016/j.physb.2022.413816.

[36] C. Du, Y. Song, S. Shi, B. Jiang, J. Yang, S. Xiao, Preparation and characterization of a novel Fe3O4-graphene-biochar composite for crystal violet adsorption, Sci. Total Environ. 711 (2020), 134662, https://doi.org/10.1016/j.scitotenv.2019.134662.

[37] M.V. Bracamonte, L.F. Venosta, W. Gustavo Fano, S.E. Jacobo, P.G. Bercoff, Graphite/nickel nanoparticle composites prepared by soft chemical methods, J. Phys. Chem. Solid. 160 (2022), 110349, https://doi.org/10.1016/j.jpcs.2021.110349.

[38] A.S. Abdulkareem, W.A. Hamzat, J.O. Tijani, T.C. Egbosiuba, S. Mustapha, O.K. Abubakre, B.O. Okafor, A.K. Babayemi, Isotherm, kinetics, thermodynamics and mechanism of metal ions adsorption from electroplating wastewater using treated and functionalized carbon nanotubes, J. Environ. Chem. Eng. 11 (2023), 109180, https://doi.org/10.1016/j.jece.2022.109180.

[39] T. Rohani, S.Z. Mohammadi, A. Beheshti-Marnani, H. Taghizadeh, Cobalt nanoparticles introduced to activated carbon, CoNP/AC, as an effective electrocatalyst for oxidation and determination of methanol and ethanol, Int. J. Hydrogen Energy 47 (2022) 6837–6847, https://doi.org/10.1016/j.ijhydene.2021.12.063.

[40] A. Rebekah, S. Sivaselvam, C. Viswanathan, D. Prabhu, R. Gautam, N. Ponpandian, Magnetic nanoparticle-decorated graphene oxide-chitosan composite as an efficient nanocarrier for protein delivery, Colloids Surfaces A Physicochem. Eng. Asp. 610 (2021), 125913, https://doi.org/10.1016/j.colsurfa.2020.125913.

[41] S. Aliyu, A.S. Ambali, T.J. Oladejo, S. Mustapha, T.C. Egbosiuba, S.O. Bada, Development of Ag-doped on multi-walled carbon nanotubes for the treatment of fish pond effluent, Reg. Stud. Mar. Sci. 58 (2023), 102797, https://doi.org/10.1016/j.rsma.2022.102797.

[42] S. Tasharrofi, Z. Rouzitalab, D.M. Maklavany, A. Esmaeili, M. Rabieezadeh, M. Askarieh, A. Rashidi, H. Taghdisian, Adsorption of cadmium using modified zeolite-supported nanoscale zero-valent iron composites as a reactive material for PRBs, Sci. Total Environ. 736 (2020), https://doi.org/10.1016/j.scitotenv.2020.139570.

[43] V. Arumugam, K.G. Moodley, A. Dass, R.M. Gengan, D. Ali, S. Alarifi, M. Chandrasekaran, Y. Gao, Ionic liquid covered iron-oxide magnetic nanoparticles decorated zeolite nanocomposite for excellent catalytic reduction and degradation of environmental toxic organic pollutants and dyes, J. Mol. Liq. 342 (2021), 117492, https://doi.org/10.1016/j.molliq.2021.117492.

[44] M. Khodadadi, A. Malekpour, M. Ansaritabar, Removal of Pb (II) and Cu (II) from aqueous solutions by NaA zeolite coated magnetic nanoparticles and optimization of method using experimental design, Microporous Mesoporous Mater. 248 (2017) 256–265, https://doi.org/10.1016/j.micromeso.2017.04.032.

[45] Q. Xu, W. Li, L. Ma, D. Cao, G. Owens, Z. Chen, Simultaneous removal of ammonia and phosphate using green synthesized iron oxide nanoparticles dispersed onto zeolite, Sci. Total Environ. 703 (2020), https://doi.org/10.1016/j.scitotenv.2019.135002.

[46] O. Eljamal, T. Shubair, A. Tahara, Y. Sugihara, N. Matsunaga, Iron based nanoparticles-zeolite composites for the removal of cesium from aqueous solutions, J. Mol. Liq. 277 (2019) 613–623, https://doi.org/10.1016/j.molliq.2018.12.115.

[47] N. Dasgupta, S. Ranjan, C. Ramalingam, Applications of nanotechnology in agriculture and water quality management, Environ. Chem. Lett. 15 (2017) 591–605, https://doi.org/10.1007/s10311-017-0648-9.

[48] A.S. Kovo, A.S. Abdulkareem, O.D. Adeniyi, M.D. Yahya, A.S. Kovo, A.S. Abdulkareem, O.D. Adeniyi, M.D. Yahya, Development of nano-silver doped zeolite A synthesized from Nigerian Ahoko kaolin for treatment of wastewater of a typical textile company Development of nano-silver doped zeolite A synthesized from Nigerian Ahoko kaolin for treatment of wastewater of a t, Chem. Eng. Commun. (2019) 1–24, https://doi.org/10.1080/00986445.2019.1641490, 0.

[49] APHA, Standard Methods for the Examination of Water and Wastewater, 23rd ed., American Public Health Association, 2017.

[50] M. Mohsin, I.A. Bhatti, M. Iqbal, S. Naz, A. Ashar, J. Nisar, F.F. Al-Fawzan, S.A. Alissa, Oxidative degradation of erythromycin using calcium carbonate under UV and solar light irradiation: condition optimized by response surface methodology, J. Water Proc. Eng. 44 (2021), 102433, https://doi.org/10.1016/j.jwpe.2021.102433.

[51] R.K. Patel, R. Shankar, P. Khare, P. Mondal, Treatment of sugar industry wastewater in continuous electrochemical process followed by low-cost adsorbent bed: performance evaluation and economic analysis, Separ. Purif. Technol. 271 (2021), 118874, https://doi.org/10.1016/j.seppur.2021.118874.

[52] J. Jose, L. Philip, Continuous flow pulsed power plasma reactor for the treatment of aqueous solution containing volatile organic compounds and real pharmaceutical wastewater, J. Environ. Manag. 286 (2021), https://doi.org/10.1016/j.jenvman.2021.112202.

[53] T.L. Adewoye, O.O. Ogunleye, A.S. Abdulkareem, T.O. Salawudeen, J.O. Tijani, Optimization of the adsorption of total organic carbon from produced water using functionalized multi-walled carbon nanotubes, Heliyon 7 (2021), e05866, https://doi.org/10.1016/j.heliyon.2020.e05866.

[54] WHO, Guidelines for Drinking-Water Quality, fourth ed., 2017, p. 631, https://doi.org/10.1016/S1462-0758(00)00006-6.

[55] 2012 US EPA, US Environmental Protection Agency, Of the Drinking Water Standards and Health Advisories, Drink. Water Stand. Heal. Advis, 2012, pp. 2–6, 2012 EPA 822-S-12-001.

[56] U. Kumari, A. Mishra, H. Siddiqi, B.C. Meikap, Effective defluoridation of industrial wastewater by using acid modified alumina in fixed-bed adsorption column: experimental and breakthrough curves analysis, J. Clean. Prod. 279 (2021), 123645, https://doi.org/10.1016/j.jclepro.2020.123645.

[57] T.C. Egbosiuba, A.S. Abdulkareem, A.S. Kovo, E.A. Afolabi, J.O. Tijani, M. Auta, W.D. Roos, Ultrasonic enhanced adsorption of methylene blue onto the optimized surface area of activated carbon: adsorption isotherm, kinetics and thermodynamics, Chem. Eng. Res. Des. 153 (2020) 315–336, https://doi.org/10.1016/j.cherd.2019.10.016.

[58] F. Feizi, A.K. Sarmah, R. Rangsivek, Adsorption of pharmaceuticals in a fixed-bed column using tyre-based activated carbon: experimental investigations and numerical modelling, J. Hazard Mater. 417 (2021), 126010, https://doi.org/10.1016/j.jhazmat.2021.126010.

[59] Y. Liu, Q. Gao, C. Li, S. Liu, K. Xia, B. Han, C. Zhou, Effective coating of crosslinked polyethyleneimine on elastic spongy monolith for highly efficient batch and continuous flow adsorption of Pb(II) and acidic red 18, Chem. Eng. J. (2019), 123610, https://doi.org/10.1016/j.cej.2019.123610.

[60] T.C. Egbosiuba, A.S. Abdulkareem, Highly efficient as-synthesized and oxidized multi-walled carbon nanotubes for copper(II) and zinc(II) ion adsorption in a batch and fixed-bed process, J. Mater. Res. Technol. 15 (2021) 2848–2872, https://doi.org/10.1016/j.jmrt.2021.09.094.

[61] K.C. Lai, B.Y.Z. Hiew, W.T. Tee, S. Thangalazhy-Gopakumar, S. Gan, L.Y. Lee, Usage of a new macro-hierarchical graphene sponge in batch adsorption and packed column configuration for efficient decontamination of cadmium in aqueous environment, J. Environ. Chem. Eng. 9 (2021), 106057, https://doi.org/10.1016/j.jece.2021.106057.

[62] D.S.P. Franco, J.L.S. Fagundes, J. Georgin, N.P.G. Salau, G.L. Dotto, A mass transfer study considering intraparticle diffusion and axial dispersion for fixed-bed adsorption of crystal violet on pecan pericarp (Carya illinoensis), Chem. Eng. J. 397 (2020), 125423, https://doi.org/10.1016/j.cej.2020.125423.

[63] J. Ifthikar, I.I. Shahib, L. Sellaoui, A. Jawad, M. Zhao, Z. Chen, Z. Chen, pH tunable anionic and cationic heavy metal reduction coupled adsorption by thiol cross-linked composite: physicochemical interpretations and fixed-bed column mathematical model study, Chem. Eng. J. 401 (2020), https://doi.org/10.1016/j.cej.2020.126041.

[64] L. Zhang, W. Niu, J. Sun, Q. Zhou, Efficient removal of Cr(VI) from water by the uniform fiber ball loaded with polypyrrole: static adsorption, dynamic adsorption and mechanism studies, Chemosphere 248 (2020), 126102, https://doi.org/10.1016/j.chemosphere.2020.126102.

[65] D.K. Singh, V. Kumar, S. Mohan, D. Bano, S.H. Hasan, Breakthrough curve modeling of graphene oxide aerogel packed fixed bed column for the removal of Cr (VI) from water, J. Water Proc. Eng. 18 (2017) 150–158, https://doi.org/10.1016/j.jwpe.2017.06.011.

[66] H. Rani, S. Prakash, T. Prasad, M. Sajid, M. Israil, A. Kumar, In-vitro catalytic , antimicrobial and antioxidant activities of bioengineered copper quantum dots using Mangifera indica (L.) leaf extract, Mater. Chem. Phys. 239 (2020), 122052, https://doi.org/10.1016/j.matchemphys.2019.122052.

[67] H. Kolya, T. Kuila, N. Hoon, J. Hee, Bioinspired silver nanoparticles/reduced graphene oxide nanocomposites for catalytic reduction of 4-nitrophenol , organic dyes and act as energy storage electrode material, Composites Part B. 173 (2019), 106924, https://doi.org/10.1016/j.compositesb.2019.106924.
[68] R.O. Ybañez-julca, D. Asunci, I.M. Quispe-d, J. Palacios, B. Jorge, M.J. Simirgiotis, S. Perveen, C.R. Nwokocha, F. Cifuentes, A. Paredes, Metabolomic profiling of mango (Mangifera indica linn) leaf extract and its intestinal protective effect and antioxidant activity in different biological models, Molecules 25 (2020) 2–19, https://doi.org/10.3390/molecules25215149.
[69] N. Sazali, Z. Harun, F. Hafeez, S. Syamsol, R. Puteri, N. Adibah, R. Ahmad, R. Hussin, N. Misdan, Materials Today : proceedings the effect of various molarity sodium hydroxide (NaOH) on the hydrosodalite formation from synthesis of Johor Kaolin , Malaysia by hydrothermal method, Mater, Today Proc 46 (2021) 2045–2051, https://doi.org/10.1016/j.matpr.2021.03.135.
[70] A. Marsh, A. Heath, P. Patureau, M. Evernden, P. Walker, Microporous and Mesoporous Materials A mild conditions synthesis route to produce hydrosodalite from kaolinite , compatible with extrusion processing, Microporous Mesoporous Mater. 264 (2018) 125–132, https://doi.org/10.1016/j.micromeso.2018.01.014.
[71] A.S. Kovo, S.M. Holmes, Effect of aging on the synthesis of kaolin-based zeolite Y from Ahoko Nigeria using a novel metakaolinization technique effect of aging on the synthesis of kaolin-based zeolite Y from Ahoko Nigeria using a novel metakaolinization technique, J. Dispersion Sci. Technol. (2010) 37–41, https://doi.org/10.1080/01932690903210218.
[72] M. Shahrashoub, S. Bakhtiari, The efficiency of activated carbon/magnetite nanoparticles composites in copper removal: industrial waste recovery, green synthesis, characterization, and adsorption-desorption studies, Microporous Mesoporous Mater. 311 (2021), 110692, https://doi.org/10.1016/j.micromeso.2020.110692.
[73] M.T. Shah, E. Alveroglu, Synthesis and characterization of magnetite nanoparticles having different cover layer and investigation of cover layer effect on the adsorption of lysozyme and bovine serum albumin, Mater. Sci. Eng. C 81 (2017) 393–399, https://doi.org/10.1016/j.msec.2017.08.033.
[74] I. Ahmad, W.A. Siddiqui, T. Ahmad, Synthesis and characterization of molecularly imprinted magnetite nanomaterials as a novel adsorbent for the removal of heavy metals from aqueous solution, J. Mater. Res. Technol. 8 (2019) 4239–4252, https://doi.org/10.1016/j.jmrt.2019.07.034.
[75] M.T. Vu, M.T. Noori, B. Min, Magnetite/zeolite nanocomposite-modified cathode for enhancing methane generation in microbial electrochemical systems, Chem. Eng. J. 393 (2020), 124613, https://doi.org/10.1016/j.cej.2020.124613.
[76] C. Pizarro, M. Escudey, E. Caroca, C. Pavez, G.E. Zúñiga, Evaluation of zeolite, nanomagnetite, and nanomagnetite-zeolite composite materials as arsenic (V) adsorbents in hydroponic tomato cultures, Sci. Total Environ. 751 (2021), 141623, https://doi.org/10.1016/j.scitotenv.2020.141623.
[77] E.F. Aboelfetoh, M.E. Zain Elabedien, E.Z.M. Ebeid, Effective treatment of industrial wastewater applying SBA-15 mesoporous silica modified with graphene oxide and hematite nanoparticles, J. Environ. Chem. Eng. 9 (2021), 104817, https://doi.org/10.1016/j.jece.2020.104817.
[78] P. Mishra, K. Singh, U. Dixit, Adsorption, kinetics and thermodynamics of phenol removal by ultrasound-assisted sulfuric acid-treated pea (Pisum sativum) shells, Sustain. Chem. Pharm. 22 (2021), 100491, https://doi.org/10.1016/j.scp.2021.100491.
[79] O.C. Iheanacho, J.T. Nwabanne, C.C. Obi, C.E. Onu, Packed bed column adsorption of phenol onto corn cob activated carbon: linear and nonlinear kinetics modeling, S. Afr. J. Chem. Eng. 36 (2021) 80–93, https://doi.org/10.1016/j.sajce.2021.02.003.
[80] N. Fallah, M. Taghizadeh, Continuous fixed-bed adsorption of Mo(VI) from aqueous solutions by Mo(VI)-IIP: breakthrough curves analysis and mathematical modeling, J. Environ. Chem. Eng. 8 (2020), 104079, https://doi.org/10.1016/j.jece.2020.104079.
[81] M. Babazadeh, H. Abolghasemi, M. Esmaeili, A. Ehsani, A. Badiei, Comprehensive batch and continuous methyl orange removal studies using surfactant modified chitosan-clinoptilolite composite, Separ. Purif. Technol. 267 (2021), https://doi.org/10.1016/j.seppur.2021.118601.
[82] T.N. Ang, B.R. Young, M. Taylor, R. Burrell, M.K. Aroua, S. Baroutian, Breakthrough analysis of continuous fixed-bed adsorption of sevoflurane using activated carbons, Chemosphere 239 (2020), 124839, https://doi.org/10.1016/j.chemosphere.2019.124839.
[83] M. Auta, B.H. Hameed, Chitosan – clay composite as highly effective and low-cost adsorbent for batch and fixed-bed adsorption of methylene blue, Chem. Eng. J. 237 (2014) 352–361, https://doi.org/10.1016/j.cej.2013.09.066.
[84] M.E. González-López, A.A. Pérez-Fonseca, M. Arellano, C. Gómez, J.R. Robledo-Ortíz, Fixed-bed adsorption of Cr(VI) onto chitosan supported on highly porous composites, Environ. Technol. Innovat. 19 (2020), 100824, https://doi.org/10.1016/j.eti.2020.100824.
[85] X.J. Lee, B.Y.Z. Hiew, K.C. Lai, W.T. Tee, S. Thangalazhy-Gopakumar, S. Gan, L.Y. Lee, Applicability of a novel and highly effective adsorbent derived from industrial palm oil mill sludge for copper sequestration: central composite design optimisation and adsorption performance evaluation, J. Environ. Chem. Eng. 9 (2021), 105968, https://doi.org/10.1016/j.jece.2021.105968.
[86] M.D. Yahya, H. Abubakar, K.S. Obayomi, Y.A. Iyaka, B. Suleiman, Simultaneous and continuous biosorption of Cr and Cu (II) ions from industrial tannery effluent using almond shell in a fixed bed column, Results Eng. 6 (2020), 100113, https://doi.org/10.1016/j.rineng.2020.100113.
[87] S. Bo, J. Luo, Q. An, Z. Xiao, H. Wang, W. Cai, S. Zhai, Z. Li, Efficiently selective adsorption of Pb(II) with functionalized alginate-based adsorbent in batch/column systems: mechanism and application simulation, J. Clean. Prod. 250 (2020), 119585, https://doi.org/10.1016/j.jclepro.2019.119585.
[88] M.L. Dlamini, M. Bhaumik, K. Pillay, A. Maity, Polyaniline nanofibers, a nanostructured conducting polymer for the remediation of Methyl orange dye from aqueous solutions in fixed-bed column studies, Heliyon 7 (2021), e08180, https://doi.org/10.1016/j.heliyon.2021.e08180.
[89] Y.H. Yoon, J.H. Nelson, Application of gas adsorption kinetics I. A theoretical model for respirator cartridge service life, Am. Ind. Hyg. Assoc. J. 45 (1984) 509–516, https://doi.org/10.1080/15298668491400197.
[90] G. Mokokwe, M.W. Letshwenyo, Investigation of clay brick waste for the removal of copper, nickel and iron from aqueous solution: batch and column studies, SSRN Electron. J. 8 (2022), e09963, https://doi.org/10.2139/ssrn.4044596.
[91] V. Chandanshive, S. Kadam, N. Rane, B. Jeon, J. Jadhav, S. Govindwar, In situ textile wastewater treatment in high rate transpiration system furrows planted with aquatic macrophytes and fl oating phytobeds, Chemosphere 252 (2020), 126513, https://doi.org/10.1016/j.chemosphere.2020.126513.
[92] H. Hoang, P. Quang, N. Thi, T. Ngoc, T. Thi, L. Tran, N. Bao, Fe3+ Fe2+, Co2+ as highly efficient cocatalysts in the homogeneous electro-Fenton process for enhanced treatment of real pharmaceutical wastewater, J. Water Proc. Eng. 46 (2022), 102635, https://doi.org/10.1016/j.jwpe.2022.102635.
[93] E. Gilpavas, I. Dobrosz-gómez, M.Á. Gómez-garcía, Optimization of sequential chemical coagulation - electro-oxidation process for the treatment of an industrial textile wastewater, J. Water Proc. Eng. 22 (2018) 73–79, https://doi.org/10.1016/j.jwpe.2018.01.005.
[94] C.M.B. de Araújo, G.F. Oliveira do Nascimento, G.R. Bezerra da Costa, A.M.S. Baptisttella, T.J.M. Fraga, R.B. de Assis Filho, M.G. Ghislandi, M.A. da Motta Sobrinho, Real textile wastewater treatment using nano graphene-based materials: optimum pH, dosage, and kinetics for colour and turbidity removal, Can. J. Chem. Eng. 98 (2020) 1429–1440, https://doi.org/10.1002/cjce.23712.
[95] M.M. Rahman, S.A. Sime, M.A. Hossain, M. Shammi, M.K. Uddin, M.T. Sikder, M. Kurasaki, Removal of pollutants from water by using single-walled carbon nanotubes (SWCNTs) and multi-walled carbon nanotubes (MWCNTs), Arabian J. Sci. Eng. 42 (2017) 261–269, https://doi.org/10.1007/s13369-016-2303-3.
[96] K. Wu, Y. Li, T. Liu, N. Zhang, M. Wang, S. Yang, W. Wang, P. Jin, Evaluation of the adsorption of ammonium-nitrogen and phosphate on a granular composite adsorbent derived from zeolite, Environ. Sci. Pollut. Res. 26 (2019) 17632–17643, https://doi.org/10.1007/s11356-019-05069-2.